Indo-Pacific Sea Surface Temperature Perturbations Associated with Intraseasonal Oscillations of the Tropical Convection

Jean Philippe Duvel

Laboratoire de Météorologie Dynamique, ENS, Paris, France

Jérôme Vialard

Institut de Recherche pour le Développement, Laboratoire d'Océanographie Dynamique et de Climatologie, Université Paris VI, Paris, France

Submitted to J. of Climate April 2005

Revised 14 November 2005

Accepted January 2006

Corresponding author address:
Jean Philippe Duvel
Laboratoire de Météorologie Dynamique,
ENS, 75231 Paris cedex 05
France

Abstract

The intraseasonal variability (ISV; 20-90 days) of the SST is examined using 7 years of data from the Tropical Rainfall Measuring Mission's (TRMM) Microwave Imager (TMI). The ISV of the SST is maximal in the summer hemisphere where the average mixed layer depth (MLD) is relatively small. For most regions of this summer hemisphere, additional indices (like the reddening of the SST signal relative to the surface flux variability) show that the ISV of the SST is statistically controlled by the integration of local surface forcing (heat flux and wind-driven subsurface cooling) by a nearly passive mixed layer. The large-scale organized *ISV* of the SST is then studied in more detail using an adaptation of the Local Mode Analysis (LMA) that extracts SST and surface wind perturbations associated specifically with *large-scale organized intraseasonal convective events*. At the basin scale, the eastward propagation of the convective perturbation is evident only over the Indian Basin. On the average, the perturbation of the surface wind tends to be maximal to the west of the convective perturbation (like for a Gill-type dynamical response), giving a primary role of the wind in the surface fluxes perturbation for region located to the west of the basin (northwest Arabian Sea and northwest Pacific Ocean). Locally, the wind perturbation (i.e. turbulent fluxes perturbation) generally lags the local convection (i.e. perturbation of surface solar flux) by less than 1/4 of period. In some cases, the surface wind is in phase with the convection reinforcing intraseasonal perturbation of the surface fluxes.

During boreal winter, the SST response to these *large-scale organized intraseasonal convective events* is large and recurrent over thin mixed layer regions of the Indian Ocean between 5°S and 10°S and North of Australia. By contrast, there is little variability of the SST linked to these organized events in the western Pacific. During boreal summer the SST response is maximal over regions of thin mixed layer located north of the Bay of Bengal, in the Arabian Sea and in the China Sea. Over the Bay of Bengal there is a northward propagation of the convective perturbation but more a standing oscillation between the equator and the north part of the Bay for the SST and the surface wind. The SST minimum generally occurs around 1/4 of period after the convective maximum and it lags the surface wind maximum by less than 1/8 of period. An intriguing result is a frequently small delay between the maximum surface wind and the minimum SST. Different explanations are invoked, like a rapid cooling due to the vanishing of warm layers as soon as the wind reinforces or abrupt wind strengthening (in regard to the time delay between two intraseasonal events) giving faster than expected cooling due to vertical mixing or surface heat fluxes.

1 Introduction

The ISV of the deep convection is one of the most organized and reproducible large-scale perturbations in the Tropics with maximum amplitude over the Indo-Pacific region. Over the Indian Ocean, this ISV has a strong seasonality. During the summer monsoon, the convective perturbation propagates northward from the equator to the Indian peninsula with maximum amplitude over the Bay of Bengal (see Lawrence and Webster 2002). These summer perturbations are strongly tied to the break and active phases of the Indian summer Monsoon that modulate the seasonal mean rainfall (Webster et al. 1998; Goswami and Ajaya Mohan 2001). During winter, the maximum amplitude of the convective perturbation is located between the equator and 15°S. This perturbation propagates eastward from the West Indian Ocean to the Central Pacific. This winter variability is generally referenced as the Madden-Julian oscillation (MJO, see Madden and Julian 1994 for a review). These perturbations are associated with westerly wind bursts generating important surface flux perturbations (e.g. Weller and Anderson 1996; Duvel et al. 2004). Many studies suggest that these westerly wind bursts can also play an important role in the onset of El Niño events when they have significant amplitude along the equator in the western Pacific Ocean (e.g. McPhaden 1999; Lengaigne et al. 2002).

The mechanisms for the generation and the evolution of the intraseasonal variability of the deep convection over the Indo-Pacific region are not perfectly understood. In particular, recent modelling studies suggest that air-sea interactions could play an important role both during summer and winter (e.g. Waliser et al. 1999; Inness and Slingo 2003; Maloney and Sobel 2004). Observations also have revealed SST perturbations up to 3K in relation with the ISV of the convection in the China Sea (Kawamura 1988), in the Bay of Bengal (Sengupta and

Ravichandran 2001) and in the western Pacific (e.g. Anderson et al, 1996). Recent satellite measurement of the SST by the Tropical Rainfall Measuring Mission's (TRMM) Microwave Imager (TMI) (Wentz et al 2000) also revealed large SST perturbations during Northern Hemisphere (NH) winter 1999 in the Indian ocean (Harrison and Vecchi 2001; Duvel et al 2004, hereafter DRV). These large SST variations, identified with the TMI satellite dataset, were confirmed by in situ data in DRV. Previous studies using the Reynolds and Smith (1994) weekly SST analyses gave far smaller SST variability related to the convective ISV (e.g. Jones et al. 1998, Shinoda et al. 1998, Woolnough et al. 2000). This is due in part to the screening effect of the cloudiness that prevents the estimate of the SST by satellite measurements in the infrared atmospheric window. This screening effect is likely to reduce the estimated ISV of the SST by masking the surface cooling during convective events.

During winter 1999, an intraseasonal SST perturbation of more than 1.5K over a large region in the Indian Ocean between 5°S and 10°S was found in both in situ and TMI SST data. From this observation, Harrison and Vecchi (2001) concluded that the strong SST variations are mainly due to vertical and horizontal heat transport, the vertical exchange with the cold subsurface being more efficient during the winter season for which the thermocline is closer to the surface. However, DRV concluded on the basis of a forced oceanic GCM that, due to the shallow ocean mixed layer in this region, the atmospheric fluxes could be sufficient to explain the observed SST anomalies with the subsurface cooling remaining negligible. This interpretation is closer to the results found by Shinoda and Hendon (1998, 2001) over the western Pacific warm pool during the Tropical Ocean Global Atmosphere Coupled Ocean–Atmosphere Response Experiment (TOGA COARE) (see also Weller and Anderson 1996; Anderson et al. 1996). DRV also suggested that formation of a warm layer prior to the cooling event might contribute to enhance

the SST perturbation.

The balance between the different physical sources that can explain the strong intraseasonal SST perturbation is still unknown and is probably variable from one event to another. A strong point however is that the shallow thermocline between 5°S and 10°S, due to average Ekman pumping during NH winter, is a fundamental feature to explain these SST perturbations in the Indian Ocean. This shallow thermocline makes cold water readily available to cool the surface by vertical mixing or local upwelling but, on the other hand, it also limits strongly the depth of the mixed layer, making it more responsive to surface forcing. This surface forcing perturbation itself is due to various physical processes that may have different phasing relative to the maximum convective activity. These physical processes are mainly the screening of the solar heat flux by the cloudiness, evaporative cooling, vertical mixing and potentially Ekman pumping linked to wind bursts. DRV showed that the latitudinal position of maximum SST variability was the result of a consensus between the position of the region of maximum flux perturbation (spanning the equator) and the region where the thermocline is shallow (between 5°S and 12°S). Results of the forced OGCM also showed that the salinity perturbation induced by the strong rain under convection and the intraseasonal Ekman pumping perturbation could play some role in the large SST response by limiting the mixed layer deepening induced by the wind perturbation.

The present study aims at characterizing the SST perturbations associated with large-scale organised convective ISV events over the whole Indo-Pacific region. This study, covering the 1998-2004 period, is mainly based on the TMI measurements for the SST and on the National Oceanic and Atmospheric Administration's (NOAA) OLR dataset (Liebmann and Smith 1996) as a proxy for the tropical convective activity. In addition, in order to isolate intraseasonal convective events that are *organized at large-scale* from the background red-noise variability at

these time scales (say 20-90 days in a broad sense), we use the Local Mode Analysis (LMA) approach (Goulet and Duvel 2000; Duvel et al 2004). A multivariate LMA is developed here in order to extract SST and surface wind perturbations related specifically to large-scale organized convective perturbations. This approach will thus also filter out the ISV of the SST linked to oceanic internal variability such as Tropical Instability Waves in the eastern equatorial Pacific and Atlantic oceans (e.g. Chelton et al 2000) or the "26-day variability" in the western equatorial Indian ocean (eg Tsai et al 1992, Kindle and Thomson 1989).

In section 2 presents the data sources and the new LMA approach (see also the Appendix) used to extract the large-scale organized convective events and the associated variability in other fields (SST and surface wind). In Section 3, the spatial distribution of the ISV of the SST and its relation to atmospheric forcing and MLD are examined and suggest a primary role of the surface fluxes in the ISV of the temperature of the mixed layer. This is further tested by looking at the reddening of the ISV of the SST in two frequency bands using a simplified relation that considers the ISV of the atmospheric forcing and a climatological MLD. In section 4, we use the LMA approach to extract the SST response to *large-scale organized convective intraseasonal perturbations* and we discuss the mean patterns of the ISV co-variability between the convection, the surface wind and the SST. In section 5, we take advantage of the LMA method to analyse variations in the properties of this coupled variability from one intraseasonal event to another. Examining the delay between perturbations of the convection, the surface wind and the SST in particular makes it possible to extract possible physical mechanisms for these SST perturbations at the intraseasonal time-scales. Summary and conclusion are given in section 6.

2 Analysis approach

a Datasets

The NOAA-OLR dataset (Liebmann and Smith 1996) is used as a proxy to study the perturbation of the convective activity. Surface wind and surface net heat fluxes are taken from the NCEP-DOE AMIP-II (R2) reanalysis (Kanamitsu et al. 2002). We use also a MLD climatology (de Boyer et al. 2004) produced by objective analysis of individual profiles.

The intraseasonal perturbation of the SST is estimated using the TMI dataset (Wentz et al 2000). The TMI instrument makes it possible to estimate the SST in cloudy conditions and is thus well adapted to study the link between the convection and the SST. The orbital characteristics of TRMM, the swath of the TMI instrument, and missing SST estimates due to heavy rainfall however result in some data void regions each day. To obtain a full tropical (38.5N, 38.5S) daily coverage, we have performed an interpolation by doing spatial filling and linear temporal interpolation from daily mean fields containing all the orbits projected on a 1x1° grid. Comparisons with in situ data done in DRV show that this product captures satisfactorily intraseasonal SST perturbations in the Indian Ocean during winter. Other studies (eg Sengupta et al 2001) have shown that this product is well adapted to study intraseasonal SST variability linked to the convection. The shortcoming reported in Bhat et al (2004) about the TMI SST (i.e. overestimated cooling for wind $>10 ms^{-1}$) will tend to slightly overestimate the SST variability over some regions but will not modify the statistical phase relationship obtained later in this study.

The intraseasonal standard deviation of the SST in the 20-90 day band is reported for the TMI dataset and the Reynolds and Smith (1994) dataset for comparison (Fig.1). Although similar patterns are apparent for both SST estimates, the amplitude of intraseasonal variability given by

the Reynolds and Smith (1994) dataset is notably smaller than the one measured by TMI, especially near equatorial region in the Indian Ocean. This is not surprising, since the Reynolds and Smith product is mostly based on measurements in the atmospheric infrared window for which the screening of clouds impairs the sampling of the SST variability (most likely the cold phase under convective clouds). Several comparisons with *in situ* data confirm that the Reynolds and Smith (1994) product underestimates the intraseasonal SST variability in the Indian ocean and that TMI performs better (e.g Sengupta and Ravichandran 2001, DRV). Since most previous statistical studies of the ISV of the SST related to convection used Reynolds and Smith (1994), it is useful in this paper to re-evaluate those results using the TMI dataset.

b The local mode analysis (LMA)

The Complex EOF (CEOF) is a straightforward approach to obtain a single manageable pattern (i.e. one complex eigenvector) describing a quasi-periodic propagative perturbation such as the ISV. Since the ISV is also an intermittent phenomenon with large seasonal variation, the CEOF has to be applied on relatively short seasonal time series for which the ISV is supposed to be quite homogeneous (i.e. for example December to April). The first shortcoming of this approach is the end effect problem inherent to the use of spectral techniques on short time series. These end effects must be reduced by a windowing (i.e. Welch window) but this will truncate/reduce the signal toward the edge of the series and thus reduce perturbations at the beginning and the end of the selected season (the ISV perturbations do not necessarily append in mid season). Increasing the size of the window to overcome this problem however induces a risk of mixing between patterns characteristics of different seasons (and not necessarily orthogonal and then appearing on a single component). The second shortcoming of an average CEOF approach is that, even for a given season, the different ISV events have not necessarily similar

patterns. The pattern obtained from an average CEOF analysis is thus not necessarily representative of the different ISV events.

The Local Mode Analysis (LMA) (Goulet and Duvel 2000, Duvel et al 2004) was designed to overcome these shortcomings. The technique is to perform CEOFs on a time section (120 days here) moving along the full time series with a small time step (5 days here). Local maxima of the percentage of variance explained by the CEOFs correspond to events that are well organized at large scale. Only the time sections centred on these events (the Local Modes) are then considered to construct average patterns for a given season (see the Appendix for the mathematical description of the method). This solves the first shortcoming due to the consideration of fixed calendar months or days to define the time section. Also, since the LMA extracts a pattern for each event (i.e. each Local Mode), it is possible to measure the resemblance between an average pattern and the patterns of each ISV event, and thus verify how this average pattern is representative of the various events in the considered time series.

The LMA technique is further developed in this paper in order to perform multivariate analysis. Using the CEOF approach, it is indeed possible to compute from one reference parameter (the OLR here) a complex eigenvector under the form of a normalized spectrum (i.e. a "spectral key"). The projection of the Fourier coefficients of all parameters (OLR, SST and surface wind) on this normalized spectrum will give the associated patterns for those fields. These patterns thus represent *SST and wind perturbations associated to large-scale organized perturbations of the convection* (OLR). Using such an approach, it is also possible (see Appendix) to extract the patterns of the average response of SST and wind to large-scale organized OLR intraseasonal perturbations (section 4). The LMA method gives a metric to compare the average pattern to the patterns of individual events. Indeed, the LMA extracts the

characteristics of the perturbations (eg timescale, phase lag between parameters, spatial patterns) for each event (section 5). This also makes it possible to study in detail the variability of the ISV events from one season (or one year) to the other.

In the following, the LMA approach is used on the OLR, SST and surface wind time series with a time window of 120 days. An analysis is performed every 5 days and only the harmonics 1 to 6 are considered (i.e. $20 \leq T \leq 120$). Prior to the analysis, in order to remove low frequencies (mainly due to the seasonal cycle), harmonics 1 to 21 are removed from the full time series (2546 days between 12 December 1997 and 30 November 2004). For seasonal statistical analyses, a local mode is selected for a given month if the date of the centre of its time sections is in this month.

c Illustration of the multivariate LMA analysis

An illustration of the LMA approach is given on Fig.2 and Fig.3 for a rather strong intraseasonal event during summer 2000 that was already reported in Vecchi and Harrison (2002). The event is a remarkable northward propagation of convective perturbations from 5°S to 20°N in the Bay of Bengal and in the East Arabian Sea (Fig.2a). This northward propagation may be seen from the progressive shift of the relative phase of the $\tilde{Z}_p^m(x)$ between adjacent regions. This multivariate pattern is the most representative for the Bay of Bengal and the Arabian Sea for which the Regional Representation Index (RRI) is larger than 0.8 for the OLR, the SST and the module of the surface wind. The delay between the minimum OLR (maximum convective activity) and the minimum SST is generally between 1/8 and 1/4 of the period (i.e. 3.5 to 7 days). The OLR-related surface wind perturbation is a maximum in the Arabian Sea and in the Bay of Bengal. The delay between the maximum surface wind and the minimum SST is smaller than 1/8 of period (i.e. 3.5 days) for most regions. For some regions in the centre of the Bay of Bengal, the

maximum surface wind is even simultaneous with the minimum SST.

This is further illustrated on Fig.3a by the reconstructed time series (Eq.A4) for a single region (15°N, 87.5°E) in the North Bay of Bengal (the declining amplitude toward the limits of the time series is due to the Welch window.) There are increases of the percentage of variance (Fig.3e) in early July for both the SST and the surface wind, showing a strong reinforcement of the *large-scale organized perturbations of these parameters* in relation with the intraseasonal convective perturbation. These large-scale perturbations described by the patterns of Fig.2, corresponds over the Bay of Bengal to a maximum OLR (i.e. a monsoon break) near the end of July 2000 flanked by two convectively active periods. Locally, this break follows a positive wind anomaly and a negative SST anomaly that are generated by the convective perturbation in mid-July. During the break, the wind decreases and the SST rises. The development of the following convective phases in August 2000 is slower with a progressive strengthening of the surface winds and a cooling of the surface. This evolution of the perturbation is in good agreement with the analysis of Vecchi and Harrison (2002). It is interesting to notice that the apparently slow development of the convectively active phase is in fact related to a short break of 10 days around 15 August, associated locally to a wind break (Fig.3d) and to a small positive perturbation of the surface temperature. There is indeed a relatively intense synoptic variability over this region of the Bay of Bengal with time-scales of 4-10 days, even for the period of suppressed convection at lower frequency (Fig.3b and 3d). However, only the slower ISV of convection and wind has a significant effect on the SST (Fig.3c) (that is consistent with the reddening of the ISV of the SST in regard to the ISV of the surface flux forcing studied in the next section).

This illustration shows that, for a relatively short time section extracted by the LMA and centered on the event, the time series of the 1st CEOF is well representative of the intraseasonal

perturbation of the three parameters (the results of Fig.3 are also valid for other regions). In particular, the phase difference between the ISV of the three parameters is well described by this Local Mode. By contrast, an average mode will give a single pattern for all events and the associated time series may be not adapted for a given region and event, giving potentially wrong phase relationships between parameters for this region and this event. The LMA thus makes it possible to analyze average patterns, that give a general view of the phenomenon, but also individual events that give the local characteristics that can be compared to the average pattern. By projecting the ISV of the SST onto OLR Local Modes extracted by the LMA, the part of the SST variability related to the large-scale organised perturbation of the convection is extracted with no *a priori* on the location of this convective perturbation.

3 Average ISV of the SST and its link to atmospheric forcing and MLD

a Average seasonal ISV of SST and atmospheric forcing

As expected (see, for example, Zhang and Dong 2004), the *convection* and the ISV of the convection are maximal south of the equator during the January-March (JFM) season (Fig.4a). The maximum ISV is generally located south of the ITCZ with minimum values over continental regions and islands. There is a strong ISV of the *surface wind* north of Australia in the Timor and Arafura Seas and in the Gulf of Carpentaria with a stronger variability (both in wind and convection) over the Ocean compared to the adjacent Australian continent. The ISV of the *SST* is particularly strong north of Australia and also in the 5°S-10°S band in the western and central Indian Ocean. There is no obvious co-location between maximum ISV of the OLR (also a proxy of the solar heat flux perturbation), the surface wind (a proxy for turbulent heat flux perturbation

and for sub-surface cooling due to vertical mixing) and SST, except north of Australia.

In JJA, the ISV of the *convection* is also maximal on the edge of the ITCZ, suggesting that the ISV plays an important role in the extension of the convective activity around the main centers of instability. In the Indian Ocean, maximum convection is found over the northeastern Bay of Bengal (contours of Fig.4e) and maximum ISV of the convection is located around the Indian Sub-continent (with a relative minimum on continental regions) and near the equator east of 70°E. The ISV of the *surface wind* is maximal in the northwest Pacific Ocean and there are two secondary maxima in the Bay of Bengal and in Arabian Sea. The ISV of the *SST* is strong north of the Bay of Bengal and on the Arabian coast. The Arabian coast is an upwelling area known for a strong eddy activity that may explain part of this variability. The region of strong ISV of the SST north of the equator in the central Pacific is also due to oceanic internal variability (tropical instability waves, see e.g. Chelton et al. 2000). The largest ISV of the SST is obtained in the western Pacific north of 20°N.

These quite complex patterns for both summer and winter seasons show that the interaction between the OLR and the SST at the intraseasonal time scales is not related only to the local perturbation of the surface fluxes by the convective systems. One must certainly consider the depth of the ocean mixed layer, as shown in the following section, and the response of the surface wind to the large-scale convective perturbation that perturbs the surface fluxes even in remote regions. The existence or not of both local and remote perturbations of the surface fluxes over the same region and the time lag between these perturbations will have an obvious impact on the final amplitude of the SST perturbation.

b Mixed layer depth and the intraseasonal SST variability

A large part of the intraseasonal variability of the SST is expected to be related to

perturbations of the average mixed layer temperature (another part being related to the formation of warm layers as discussed in DRV). This average mixed layer temperature varies following the equation derived from the heat conservation equation integrated vertically over the MLD, H (see e.g. Duvel at al., 2004):

$$\partial_t T = \frac{Q^* + Q_S\left(1 - f\left(-H\right)\right)}{\rho_0 C_P H} + \frac{E_{-H}}{\rho_0 C_P H} - u\partial_x T - v\partial_y T + D \qquad (1.)$$

The first term of the equation represents the heat flux forcing (Q_S is the net surface solar heat flux; Q* is the non-solar part of the heat flux, f(-H), the fraction of the solar radiation that penetrates down to the depth H, $\rho_0 C_P$ is the volumic heat capacity of seawater (4.10^6 $JK^{-1}m^{-3}$). The second term is the effect of the interior ocean (E_{-H} is the heat flux at the bottom of the mixed layer, which is a combination of entrainment, vertical mixing and effect of vertical current). The two following terms are the zonal and meridional advection by the mean mixed layer currents. The last term stands for the (usually small) effects of current vertical shear in the mixed layer and effects of lateral eddy heat flux convergence.

In this equation, H is thus a key factor controlling the reactivity of the mixed layer temperature to either surface heat fluxes or heat exchange at its bottom. Outside the equatorial zone, these bottom exchanges are mostly cooling related to surface forcing, either dynamically via wind stress or thermodynamically by the generation of negative buoyancy of the surface layer. The vertical current term will be also forced in part by Ekman pumping generated by the surface wind stress.

Without precise information on the variability of the mixed layer structure, it is difficult to quantify the role of the different physical processes of (1) in the ISV of the SST. However, in a first approach, the influence of the MLD on the intraseasonal variability of the SST may be

investigated by comparing average maps of MLD and intraseasonal variability of the SST for winter (JFM; Fig.4c and 4d) and summer (JJA; Fig.4g and 4h). These maps are indeed remarkably similar with generally a maximum ISV of the SST for small values of the MLD. This suggests that the first two terms of (1) represent essential processes for the ISV of the SST. A striking feature is the band of strong intraseasonal variability between 5°S and 10°S in the Indian Ocean in JFM in a region of thin (20-30m) mixed layer, in good consistency with the two events studied in detail in Duvel et al (2004). Also, the region of large ISV of the SST below the SPCZ is associated with a 20-30m mixed layer. During summer, regions of strongest ISV of the SST correspond to thin mixed layer such as in the South China Sea, in the western Pacific subtropics, in the northern Bay of Bengal and western Arabian Sea. This qualitative assessment is confirmed by the rather high (0.67 for JFM and 0.74 for JJA) linear correlation coefficient between maps of the ISV of the SST and the inverse of the climatological MLD. This result shows in addition that the MLD climatology is apparently sufficiently robust to represent the broad seasonal distribution of the MLD for the 1997-2004 period.

This suggests that the first two terms of (1) represent a main source of ISV for the SST. This is in good agreement with previous studies (e.g. Jones et al. 1998, Shinoda et al. 1998, Woolnough et al. 2000, Duvel et al. 2004) showing that the first term, i.e. the effect of the net surface heat flux, is the dominant term in the ISV of the SST. For regions with an ISV controlled primarily by this first term, one may expect a good correlation between the derivative of the SST and the net surface heat flux forcing. These regions are identified in the following by computing such a correlation in two spectral bands by using the net surface flux provided by NCEP re-analyses. We thus consider that the net surface fluxes given by the NCEP re-analysis are precise enough to give the correct intraseasonal phase and amplitude. This hypothesis is somewhat justified *a posteriori*

by the significant correlation obtained in the 30-90 day band (Fig.5a and 5c) and the 20-30 day band (Fig.5b and 5d). These two intraseasonal bands correspond to the same number of harmonics of our time series of 2546 points, 49 harmonics for the "30-90" day band (29-78) and for the "20-30" day band (79-128). This gives a degree of freedom of 96 for the whole time series and thus 24 for the JFM seasons and a correlation of 0.5 is thus significant at the 99% confidence level. The correlation is indeed larger than 0.5 for most regions of the summer hemisphere. For these regions, an additional diagnostic can be done to quantify the potential role of the first RHS term of (1) in the ISV of the SST. If this role is important, the variability of the SST can be approximated by a simplified relation:

$$\partial_t T = \frac{Q}{\rho_0 C_P H} \qquad (2.)$$

where Q represents the net surface fluxes. In the following, the depth H of the mixed layer is taken from the seasonal value of the de Boyer et al. (2004) climatology (Fig.4d and 4h). We thus consider that interannual and intraseasonal variabilities of the MLD have only little impact on the general correlation. This last point is certainly wrong in the highly reactive equatorial region but may be considered acceptable in other regions, as shown in Duvel et al (2004) for the Indian Ocean during NH winter. For a pulsation ω, (2) becomes:

$$\partial_t T = \frac{\sqrt{2}\,\sigma_Q^{\omega}\cos(\omega t)}{\rho_0 C_P H} \qquad (3.)$$

where σ_Q^{ω} is the standard deviation of Q for this spectral band. Integrating (3), the standard deviation of the SST variability induced by the forcing at pulsation ω is:

$$\sigma_T^{\omega} = \frac{\sigma_Q^{\omega}}{\rho_0 C_P H \omega} \qquad (4.)$$

The regions for which the fisrt term of (1) is the main processes of the intraseasonal variability

should thus verify equation (4). As reported in Hasselman (1976), the presence of the pulsation ω at the denominator in (4) translates the variance toward low frequencies giving a reddening of the spectrum. This reddening can be verified by estimating σ_T^ω and σ_Q^ω from the TMI and NCEP datasets, respectively. Based on (4), a linear relation $\sigma_T^\omega = c_\omega \sigma_Q^\omega / H + n$ is expected between σ_T^ω and σ_Q^ω / H for a given ω with a corresponding characteristic time scale $\tau = 2\pi\rho_0 C_P c_\omega$. The constant n represents the SST variability due to sources independent of the surface flux. The linear shape of the relation between σ_T^ω and σ_Q^ω / H for two different frequency bands appear to be quite robust taking into account the use of completely independent datasets. In the 20-30 day band, the timescale τ estimated from the linear regression is 26.5 days for JFM (Fig.5f) and 29 days for JJA (Fig.5h). In the 30-90 day band it is 43.3 days for JFM (Fig.5e) and 53.4 days for JJA (Fig.5g). The good consistency between the period τ deduced from the slope c_ω and the input spectral domain of σ_T^ω and σ_Q^ω confirms the statistical reddening of the SST spectrum consistent with a mixed layer integrating the surface fluxes variability for the considered regions. This is consistent with the hypothesis that for most regions of the summer hemisphere, the surface fluxes are statistically a leading source of SST variability at intraseasonal timescales. However, as shown by the dispersion of the scatter diagrams on Fig.5, this statistical relation does not preclude other atmospheric-driven processes, like turbulent mixing at the mixed layer bottom, formation of warm layers or Ekman pumping to also play a role in the ISV of the SST.

The above estimates of the ISV of the SST and wind did not isolate the part that is specifically linked to *large-scale organized ISV of the convection* (like the MJO during NH winter). In the Indo-Pacific region, a large part of the intraseasonal forcing is indeed due to a succession of quasi-periodic events that will strongly organize the ISV of the whole coupled system (in this case the reddening for a quasi-periodic event will slightly translate the amplitude of the peak in

the SST spectrum toward lower frequencies.) For this organized ISV, the formation of warm layers and/or Ekman pumping may play a more important role in the perturbation of the SST. Extracting these organized intraseasonal perturbations will thus give more information on the origin of the ISV of the SST and on its potential feedback on the atmosphere. The ISV is however an intermittent phenomenon and, as shown in the previous section, one must build the relation between the SST and the OLR on an index based on the large-scale organisation of the convection rather than only on the local OLR perturbation. To understand the physical source of the intraseasonal SST response, it is thus certainly adapted to use an approach such as the multivariate LMA. This makes it possible to extract the SST and wind perturbations for each intraseasonal event as a function of the OLR large-scale organized perturbations.

4 ISV of the SST associated to large-scale organised convective perturbations

As shown in Goulet and Duvel (2000), seasonal average patterns for the whole Indo-Pacific area are poorly representative of individual events, especially during boreal summer. Thus, while some intraseasonal events are well organized over the whole Indo-Pacific region, there are also a variety of events that are organized only at the basin scale. In addition, we are interested here mostly by the relation between the convection, the surface wind and the SST and not by the inter-basin structure of the convective perturbations. The large-scale organized convective events are thus detected here by applying the LMA separately for the Indian Ocean (50°E-110°E, 30°S-30°N), the Maritime Continent (100°E-160°E, 30°S-30°N) or the western Pacific (150°E-210°E, 30°S-30°N).

The NCEP radiative surface fluxes are not used here because we prefer to rely on the observed

OLR as a proxy for the phasing between the SST and the solar flux perturbation due to deep convection. Also, the NCEP surface wind is used instead of the surface turbulent flux in order to have more direct information on the other potential role of the wind in SST perturbations related for example to upwelling, mixing with subsurface water or warm layer formation. The analysis of the phase relation between the OLR, the surface wind and SST can bring information on the processes at work. For example, if convection and wind perturbations are in-phase, one expects a 1/4 period lag of the SST with respect to these perturbations if surface fluxes are the dominant process. The phase relation between the wind and the SST due to other processes is however more variable in regard to his lag of 1/4 of period related the simple integration of surface fluxes by a mixed layer with constant depth. For example, in presence of a warm layer prior to the convective perturbation, the daily mean SST will tend to be maximal for the minimum wind and will sharply decrease toward the average mixed layer temperature as soon as the wind rise above a given threshold. Even if the mixed layer temperature then evolves under the forcing of surface fluxes, the phase relationship between wind and SST will be modified by this warm layer formation/destruction with a SST becoming more in phase opposition with the surface wind.

a Indian Ocean

Some characteristics of the OLR intraseasonal events detected over the Indian Ocean area are first shown on Fig.6. There is a clear seasonal variation of the average standard deviation (Fig.6a) of the events with minimum value for the few events around the equinoxes. The standard deviation of the Local Modes is maximal in January and May. A striking feature is the bloc of strong events in May that are quite separated from a bloc of event for the mid-June to mid-August (there is no event detected in September). For NH summer months, we will thus examine separately May corresponding to the season of pre-onset and “bogus” onset (Flatau et al 2001)

and JJA corresponding to the core months of the monsoon. The average patterns are thus computed on 7 events in JFM, 10 events in JJA and 6 events in May. There are in fact two very similar events in May 2004 (due to the particular time evolution of the variance percentage) but the redundant Local Mode is nevertheless conserved since it does not change significantly the average results (not shown).

Since the ISV is not purely harmonic, the "period" of an ISV event is not perfectly defined. We use here the procedure proposed in Goulet and Duvel (2000) to compute an "average time-scale" from a sum of phase differences between two time steps weighted by their average amplitude. This is done on the time series corresponding the spectrum $\tilde{\psi}_p^m(k)$. After careful examination of different events, a good approximation for the "period" of an event appears to be this "average time-scale" diminished by its standard deviation (this diminution is needed because the first harmonics considered - 120 and 90 days - tends to overestimate the "average time-scale"). The resulting period reported in Fig.6b confirms a weak tendency already highlighted in Goulet and Duvel (2000) to have shorter time-scale during NH summer. The two events of NH winter 1999 already studied in Harrison and Vecchi (2001) and DRV have a relatively short period compared to other winter events, particularly for the January 1999 event.

For JFM, the average OLR pattern (cf. Section c of the Appendix) (Fig.7a) represents a typical eastward propagating perturbation with a phase speed around 6°/day for an "average time-scale" of 35 days (Fig.6b). The maximum OLR amplitude is located south of the equator over the eastern Indian Ocean. The associated SST perturbation (Fig.7b) is also maximal south of the equator with maximum amplitude over the central Indian Ocean at 7.5°S. There is an eastward propagation of this SST perturbation with a relative phase lag of 1/8 to 1/4 of period in regard to the OLR (Fig.8a). There is also an equatorward propagation of the SST anomaly (Fig. 7b), as for

the surface wind (Fig.7c), giving a slightly longer delay (1/4 of period) between the maximum convection and the minimum SST near the equator (Fig.8a). The associated surface wind perturbation is maximal over the West Indian Ocean south of the Equator (Fig.7c). The maximum perturbation occurs less than 1/8 of period before the minimum SST and is even simultaneous with the minimum SST for regions near the Equator (Fig.8b). In regions of large SST perturbation near 7.5°S, the wind perturbation is maximal just after the convective maximum (Fig.8c). This delay between the wind maximum and the convection tends to be larger near the equator and over the Eastern Indian Ocean. For a Gill-type dynamical response to convective warming (Gill, 1980), the maximum wind perturbation (mostly westerly wind) is expected west of the convective maximum. This will introduce a lag between the convection and the wind perturbations for an eastward moving perturbation. In addition, Fig.7 shows that for the three seasons, the average ISV of the surface wind is shifted to the west in regard to the maximum OLR perturbation. This is also in agreement with a (mainly zonal) surface wind perturbation associated to a Gill-type dynamical response.

In May, the organized convective perturbation is maximal south of the Bay of Bengal (Fig. 7d). The average pattern is a northward propagation with a phase speed around 2°/day, superimposed to an eastward propagation with a propagation speed of 4-5°/day. The corresponding wind and SST perturbations are maximal south of the tip of India and over the Bay of Bengal (Fig.7e and f), in agreement with bogus onsets described in Flatau et al (2001). For most regions, the SST is minimal 1/4 of period after the maximum convection (Fig.8d) and nearly simultaneous with maximum surface wind (Fig.8e). Here, the wind is thus maximum 1/4 of period after the maximum convection (Fig.8f).

In JJA, the most striking difference compared to May is the stronger perturbation of the

convection between 10°N and 25°N over the Indian subcontinent and the eastern Arabian Sea (Fig.7g) related to enhanced perturbations for both SST and surface wind (Fig.7h and 7i). The SST amplitude is maximal northwest of the Arabian Sea over regions of small MLD (Fig.4h). The OLR amplitude over northwest Arabian Sea is weak, suggesting that the ISV of the SST is rather due to the surface wind perturbations associated to the ISV of the convection further east. According to results reported in Joseph and Sijikumar (2004) there are indeed intraseasonal perturbations of the low-level wind over the Ariabian Sea associated to convection over the Bay of Bengal (see their figures 5 and 6). Near the coast of Oman, SST and wind perturbations tend to propagate northward more slowly (around 0.6°/day) north of 15°N over the Arabian Sea but keep their phase difference of about 1/8 of period (Fig.8h). The SST perturbation there might be linked to a modulation of the upwelling by the local wind perturbation.

There are also relatively large perturbations of SST and surface wind south of the tip of India and north of the Bay of Bengal (Fig.7h and 7i). This is related to a phase opposition of the perturbations between these two regions. This phase opposition is more striking for the SST and the surface wind, and well underlined by the absence of variability around 7.5°N. Near the equator, maximum surface wind and convective activity precede the minimum SST by about 1/4 of period (Fig.8g and 8h). For the Northern Bay of Bengal, the surface wind is a maximum during or just before the minimum SST. This feature is also well illustrated for the mode of summer 2000 (Fig.2 and Fig.3), showing also the good reproducibility of this multivariate pattern. Near the equator, the wind is maximal during the convective event (Fig.8i), in agreement with the relatively large SST perturbation despite the thick mixed layer (Fig.4h). The wind perturbation over east Arabian Sea (Eq-10°N) moves northward more slowly than the local convective perturbation (Fig.7i and 8i) but at a speed close to the northward propagation of the

convective perturbation over the Bay of Bengal. This suggests that the wind perturbation over east Arabian Sea is mainly associated to a Gill-type dynamical response to the convective perturbation over the Bay of Bengal. Over the Bay of Bengal, the northward propagation of the OLR perturbation is faster during bogus onset in May (Fig.7d) compared to JJA (there is roughly 1/4 of period between the equator and 15°N in May compared to 10°N in JJA). This may explain the better agreement between the northward phase propagation of OLR and wind perturbations over the eastern Arabian Sea (Eq-10°N) in May (Fig.8f).

The location and the magnitude of the average OLR, SST and wind perturbation patterns described above are due to an ensemble of events, each being the result of a subtle combination of the local MLD, the location of the large-scale convective perturbation and its associated atmospheric dynamical response. This may lead to quite variable patterns from one intraseasonal convective event to another and thus to non-significant average patterns. By computing the distance between each pattern and the average pattern, it is however possible to test how this average perturbation pattern (A13) is representative of the ensemble of Local Modes (A3). This is illustrated on Fig.9 showing, for each parameter, the normalized distance between each Local Mode and the average pattern.

Considering the three parameters, the multivariate patterns of Fig.7 for JFM are mostly representative of year 1999, 2001 and 2002 (and 2004 in a lesser degree). For 1998 and 2000, the distance is large for the three parameters (no well organised event is detected for 2003). May and JJA average patterns are also quite representative of the ensemble of Local Modes of the corresponding season. These average patterns are less representative for years 1999, 2000 and 2001 for May, and for years 2003 for JJA. In JJA, there is a similar distance for most Local Modes and year 2000 (see section 2) has indeed ISV patterns close to the average patterns. Note

that this distance is smaller for the actual modes of a selected season compared to other season showing the specificity of these seasonal average patterns. Also, the Local Mode patterns of SST and wind are close to the average pattern when the OLR perturbation pattern is itself close to the average. This shows that the extracted multivariate average patterns are indeed the result of a reproducible coupling (or, at least, co-variability) between the three parameters.

b Maritime Continent

For this area, there is less seasonal variation of the characteristics of the Local Modes (Fig.10). It is interesting to note that while some modes are contemporaneous with the modes extracted over the Indian Ocean basin (like February 98 for example), some exist only for one basin (January and March 1999 over the Indian Ocean), and others exist for both basin but with different local characteristics (January 2002 with different time scales). Since there is nothing remarkable in May, only the JFM and JJA seasons are considered.

In JFM, the perturbation for the three parameters (Fig.11) is maximal south of the equator between 7.5°S and 15°S, off the northwest coast of Australia for a region of relatively thin mixed layer (Fig.4d). Note again the relative minimum of the perturbation over continental Australia compared to adjacent sea for both OLR and surface wind perturbations. As for Indian Ocean region, the minimum temperature is reached around 1/4 of period after the convection maximum (Fig.12a) and the delay in regard to the wind maximum is shorter with about 1/8 of period between wind maximum and SST minimum (Fig.12b). The eastward propagation is hardly visible here on the relative phase field (Fig.11a) that rather shows a southward propagation (i.e. poleward, as for summer patterns). The surface wind is maximal only shortly after the maximum convection (Fig.12c), giving a nearly in phase modulation of solar and turbulent surface fluxes that will reinforce the SST perturbation due to surface fluxes.

In JJA, the convective perturbation is maximal between the equator and 15°N and propagates northward at a speed (≈2°/day) very close to the phase speed over the Bay of Bengal at the same season (Fig.11d). The associated SST perturbation is maximal in the South China Sea (10°N, 110°E) and, more generally northwest of the maximum OLR perturbation (Fig.11e), over regions with small MLD (Fig.4h). The surface wind perturbation is also maximal on the northwest side of the OLR perturbation (Fig.11f) with maximum amplitude around 10°N. The wind perturbation is strong and moves northward faster compared to the north Indian Ocean during the same season (Fig.11f). As for the Arabian Sea, north-eastern regions have a small MLD and the SST perturbation is associated mostly with surface wind perturbation (the OLR perturbation is small and probably unrelated to deep convection). South of 10°N, the SST is minimal 1/4 of period after the maximum convection (Fig.12d). North of 10°N, the SST is rather in quadrature with the surface wind and becomes out of phase with the surface wind further south (Fig.12e). In between, around 10°N, OLR and wind perturbation are strong and out-of-phase (Fig.12f), giving a larger perturbation of the surface fluxes that may explain the larger ISV of the SST (thus in quadrature with both OLR and surface wind) here despite the relatively thick mixed layer.

These average patterns are more representative for the end of the 1998-2004 period for both the JFM and the JJA seasons (Fig.13). Average patterns for both summer and winter are more representative of years 2001, 2002 and 2004.

c Western Pacific

Excepted for boreal winter, the standard deviation of the OLR Local Modes is smaller over this region than other the previous ones (Fig.14 compared to Figs.6 and 10). As for the two other basins, the period of the perturbation is quite dispersed (Fig.14b). Some Local Modes are contemporaneous with the modes extracted over the Indian Ocean basin and the Maritime

Continent, like the Local Modes of 2002 and 2004. Due to the small amplitude for other seasons, only the JFM season is considered below.

For the nine events considered, the average OLR pattern over the western Pacific is rather a westward propagation (Fig.11g). The amplitude of the OLR perturbation is maximal south of the equator near the dateline. The corresponding perturbation of the SST is very small (Fig.11h) and located to the south of the OLR perturbation, in better correspondence with the surface wind perturbation. Minimum SST is reached generally 1/4 of period after the OLR minimum (Fig.12g) and between 1/4 and 1/8 of period after the surface wind maximum (Fig.12h). These average patterns are mostly representative of years 2002 and 2004 (Fig 15) that appears to be also the modes well organised at the Indo-Pacific scale (a mode exists in January for each basin for these years).

5 Intraseasonal phase relation for selected regions

On the basis of previous results, the delay between the perturbations of the three parameters for different intraseasonal events is explored in more details over selected regions (Fig.16). These regions are chosen because of their strong average amplitude and their relatively homogeneous phase for the average patterns of three parameters. A regional average phase lag between the parameters is computed for each multivariate Local Mode. This phase lag is expressed in days using the periods of Figs.6b, 10b and 14b. The phase lags between minimum SST, maximum surface wind and minimum OLR are presented on Fig.17.

For both the SW and the SE regions, there is a large seasonal cycle of the SST and intraseasonal events appear clearly in association with the development of the convective instability during the warmest season. For the SC region, the seasonal cycle of the SST is smaller

and there is intraseasonal OLR variability all along the year. The maximum ISV is nevertheless attained during winter months that are also the warmest season for this region. For these 3 regions, the surface wind is at a seasonal minimum during winter, excepted during intraseasonal events when the wind reaches higher values in relation with the westerly wind events.

Over the West Indian Ocean (region SW), the MLD is minimum for JFM and the intraseasonal SST perturbation is relatively large for most events despite the absence of strong OLR or surface wind perturbation. As shown in Duvel et al (2004) for the March 1999 event, the ISV of the SST over this region can also results from the vanishing of a warm layer during the convective event. The SST is minimal 2 to 8 days after the maximum of the local OLR perturbation (Fig.17a). For the two low frequency (Fig.6b) events of January 2001 and 2002, the minimum SST is nearly simultaneous with the maximum surface wind and the delay after the minimum OLR is respectively around 3 and 7 days. For the higher frequency events of January 1999 and 2000, wind and convective perturbations are nearly in phase but the delay of the minimum SST is also quite variable and not clearly related to the period of the events (Fig.6b). Similar variability of the phase relation between the three parameters is observed for the Central Indian Ocean (region SC). Here, the January 1999 event already studied in Harrison and Vecchi (2001) and DRV corresponds to a strong perturbation of the SST region that is nearly simultaneous with the maximum wind (Fig.17b). The same characteristic is observed in January 2002, showing that this strong perturbation is not a unique feature of 1999. For the SE region, strong SST perturbation in 2002 and 2004 are associated to large perturbations of both OLR and surface wind.

For the North Bay of Bengal (region BB), a large seasonal cycle of the SST and intraseasonal convective events appear clearly in association with the development of the convective instability and an increased surface wind speed (Fig.17d). This development is associated with a cooling of

the SST during the monsoon season, followed by a secondary warming in September when the convective activity and the surface wind decrease. For the intraseasonal events, the SST is minimal 4 to 10 days after the minimum OLR. The strongest SST perturbations occur in 1998, 2000, 2001 and 2004 for which two strong events are detected in June and August. For most events, as for the average pattern, the surface wind is maximal only a few days before the minimum SST. For the event of summer 2000 (already illustrated in Fig.3 but for a region of the central Bay of Bengal), the synchronized variations of SST and surface wind for these Northern regions is also evident with a lag shorter than 5 days between minimum OLR and minimum SST. Another example is shown for the Equatorial region south of the Bay of Bengal (region EQ) for May events corresponding mainly to the bogus monsoons. Here, the seasonal variation of the SST is weak and there is an ISV of the OLR all along the year. May corresponds to abrupt reinforcing surface wind and SST cooling. SST perturbations are relatively large over this region where the climatological MLD is still relatively small before the bogus monsoon onset (20-30m in April). In good agreement with the average patterns (Fig.8), the SST is minimal 5 to 10 days after the minimum OLR and nearly simultaneous with the surface wind perturbation.

6 Summary and discussion

It is important to understand the source of the large-scale organized coupling between the convection and the SST at intraseasonal time-scale for a correct representation of these processes in global models and thus for the predictability of intraseasonal events. Using available observational datasets of SST, OLR and surface wind for seven years, this study is an attempt to retrieve the main characteristics of the ISV of the SST field and to trace the source of this variability. The use of the relatively new TMI SST dataset makes it possible to analyse the ISV of

the SST with more accuracy than previous studies using the Reynolds and Smith (1994) dataset.

This study first considers the relationship between a climatological MLD and the amplitude of the ISV of the SST. For the Indo-Pacific region, there is larger ISV of the SST where the mixed layer is thinner, as expected for a slab ocean integrating passively atmospheric forcing. Applied in the intraseasonal range, the simple model of Hasselmann (1976) gives an ISV of the SST that is proportional to the ISV of the surface flux and inversely proportional to the MLD and frequency. Using climatological MLD estimates, TMI SST and NCEP surface fluxes, it is shown that this idealized model holds statistically within the 20-90 days range for most region of the summer hemisphere. This suggests that a large fraction of the ISV of the SST in the tropical Indo-Pacific results from a climatological mixed layer integrating surface forcing (heat flux or wind-driven subsurface cooling). In such a case, one may expect a larger ISV of SST not only for region with larger ISV of the surface fluxes or thinner mixed layer but also for ISV at lower frequency (the ISV of the SST will be twice as large for a 40 day oscillation of the forcing compared to a 20 day oscillation of the same amplitude).

One may question this result since several processes in (1), and in particular the intraseasonal variability of the mixed layer, are neglected in (4). However, analysis of model mixed layer variability (not shown) in the forced OGCM simulations used in DRV shows that intraseasonal variability of the mixed layer depth is small in the tropics when compared to the seasonal or interannual variability of the mixed layer depth. The only exception is for the equatorial zone. This can be understood since the zonal wind directly accelerates the zonal flow in the equatorial band, giving fast upper current changes and deepening of the mixed layer by shear. The slower dynamics at higher latitude make the currents less responsive and thus vertical shear more difficult to generate at intraseasonal timescale. This point was illustrated for two intraseasonal

events only in DRV but the underlying physic is probably also valid for other regions and events. Similarly, the deepening of the mixed layer due to Buoyancy forcing is more efficient at longer time scales than at intraseasonal timescale. Intraseasonal variability of the mixed layer is thus smaller than the seasonal or interannual variability.

Also, the diagnostic made in section 3 does not make it possible to distinguish between the role of surface heat fluxes and wind-driven subsurface cooling in the intraseasonal variability. Both are likely to contribute, but several arguments tend to show that the surface net heat flux is the dominant effect in most regions. First, several previous studies have already suggested that surface heat fluxes are dominant for MJO driven variability (e.g., Shinoda and Hendon, 1998, 2001; DRV). Second, the good statistical and quantitative consistency obtained with (4) suggests that the regional ISV of the SST variability matches well with the amplitude of the flux variability, even with a climatological MLD. Third, as suggested above, the mixed layer intraseasonal variability in most regions of the tropics is quite weak compared to e.g. the seasonal variability. This suggests that there is probably relatively weak flux variability at the bottom of the mixed layer at these timescales. However, a precise quantification of the relative role of surface heat flux and wind-driven subsurface cooling in the ISV of the SST deserves detailed studies of the upper ocean heat budget at intraseasonal timescales.

The link between the *large-scale organized ISV of the tropical convection* and the ISV of the SST is examined using an adaptation of the LMA analysis (Goulet and Duvel, 2000). This new multivariate approach is applied to determine the average patterns of SST and the surface wind perturbation related to large-scale convective events. Results show that, for the studied 1998-2004 period, seasonal average multivariate patterns at the basin scale are robust and represent around half of the intraseasonal events for a given season and a given basin (Indian Ocean,

Maritime Continent and Western Pacific). By construction, these patterns are relatively close to average CEOF patterns computed on time sections of the corresponding season. Mathematically, the only difference is that an average CEOF will be computed on fixed time sections defined from calendar days. The average LMA is also an average CEOF but is computed from the time sections previously extracted from the LMA and that are centred on large-scale organized events (and on the corresponding season). Compared to an average CEOF analysis, the LMA approach makes it possible: (i) to extract time sections centred on large-scale organized perturbations (ii) to give specific pattern and spectral characteristics for each extracted time section and, (iii) to test how the average pattern represents perturbations that succeed one another in time. The LMA applied to each basin independently extracts organized events at the basin scale that are contemporaneous for the three basins (such as for January 2002 and 2004). This inter-basin organisation is consistent with a canonical MJO perturbing the whole Indo-Pacific area. However, other events are organized at the basin-scale only suggesting that the inter-basin organisation is not a necessary condition for the existence of strong organized coupled perturbations.

During summer for the Indian Ocean, the OLR-related ISV of the SST is maximal over a region extending from the Equator up to the Northern limits of the Arabian Sea and the Bay of Bengal. The ISV patterns of the three parameters present reproducible specificities for intraseasonal events related to “bogus monsoon onsets” in May, and actual intraseasonal variations during the monsoon. During the monsoon, SST and surface wind perturbations in the Bay of Bengal present more the character of a standing oscillation between the equator and the North Bay of Bengal with minimum amplitude around 10°N. The general picture for the Arabian Sea and continental India is a wind perturbation mainly related to the development of the

convection over the Bay of Bengal in agreement with results shown in Joseph and Sijikumar (2004). Over the western Arabian Sea, the SST perturbation is mostly due to this wind perturbation and could be related in part to the associated variations of the upwelling. Compared to the JJA season, there is a faster northward propagation across the Bay of Bengal in May that is associated to an eastward propagation of the intraseasonal perturbation. The resulting wind perturbation is lagged (a quadrature) in regard to the OLR in agreement with a Gill-type dynamical response to an eastward moving convective perturbation. The picture is different for the northwestern Pacific in JJA. If the northward propagation of the convective perturbation is similar, the associated SST and wind perturbations do not exhibit the phase opposition as for JJA over the Bay of Bengal. An eastward moving of the perturbations is also hardly detectable and the surface wind perturbation propagates northward faster than the convective perturbation. The SST perturbation is maximal over northwestern region where the MLD is small and around 10°N where OLR and surface wind perturbations are out-of-phase (i.e. solar and turbulent fluxes in phase)

During boreal winter, the ISV of the OLR extends throughout most of the Indian Ocean and western Pacific. Nevertheless, the OLR-related SST and surface wind responses is large only between 5°S and 10°S over the Central Indian Ocean and off the northwest coast of Australia. The eastward propagation of the convective perturbation is clear for the Indian Ocean basin only. For most regions, the various ISV events are characterized by a minimum SST occurring 1/4 of period after the maximum convection. However, especially for some strong events over the Central Indian Ocean during winter, but also for region of central Bay of Bengal during summer, the SST is a minimum during or just after the surface wind maximum.

The fact that, even for a given region and a given season, OLR and surface wind have

different intraseasonal phase relations for different events is not surprising. This is because the response of the surface wind depends more on the timing and location of the large-scale convective perturbation than on the local convective perturbation. However, the variable delay between the maximum perturbation of the driving surface flux parameters (convective cloudiness and surface wind) and the SST is more intriguing and deserve further discussion.

If the OLR (proxy for the surface solar flux perturbations) and the surface wind (proxy for the surface turbulent heat flux) are out-of-phase (i.e. solar and turbulent flux in-phase), as for example over the northwest Pacific during JJA around 10°N (Fig.12f), and if those surface fluxes are the main source for SST perturbations, the time of their maximum perturbation should correspond to the time of maximum derivative of the SST (1). In such a case, the lag between the maximum surface fluxes and the minimum SST is of the order of 1/4 of period, as for northwest Pacific Ocean around 10°N in JJA (Fig.12e). However, as shown in the previous sections, surface wind and OLR ISV perturbations present various strength and relative phase relationship depending on region and season. In particular, for eastward moving Gill-type atmospheric perturbation, the surface wind maximum will lag the convective maximum, reducing the whole impact of the surface flux perturbation on the SST and giving a larger variety of SST-OLR and SST-wind phase relationship. Since, the wind is generally maximal between 0 and 1/4 of period after the convective maximum (Fig.8 and 12), an SST driven by surface fluxes should be theoretically minimal between 1/4 and 1/2 period after the convection maximum. An SST minimum during or just after the surface wind maximum thus means either that the surface wind does not impact the SST significantly or, on the contrary, that the surface wind strongly and rapidly cools the surface, as for example for a warm layer destruction. In addition, and this could be an important feature, the ISV is not a purely sinusoidal signal and the wind reinforcement may

be more abrupt than expected from the filtered signal. This will give a SST response (either due to surface fluxes, subsurface cooling or upwelling) in a shorter delay compared to the time-scale between two perturbations detected from the OLR. A good example is shown on fig.3d showing an abrupt wind burst after calm conditions in the beginning of July 2000 that may explain the short delay between maximum wind and minimum SST.

To conclude, despite the relatively short time series used here (7 years), this study shows relatively robust patterns for the response of both the surface wind and the SST to large-scale organized convection. This shows in particular a strong ISV of the SST south of the equator in the Indian Ocean and north of Australia during winter that is associated with a relatively thin mixed layer. This is in contrast with the weak SST response to the ISV of the convection found over the western Pacific for the seven years considered. The exact nature of the processes of the SST cooling still has to be explored in more detail, especially to understand the origin of the frequently short delay between the maximum wind and the minimum SST. To this end, detailed modelling analyses of the ocean mixed layers variability associated to in situ measurements are necessary to examine the role of different processes such as warm layers formation and sub-surface cooling. Due to the large and reproducible intraseasonal SST perturbations found here it appears more and more necessary to correctly represents this coupling in general circulation models.

Acknowledgements: TMI data are produced by Remote Sensing Systems and sponsored, in part, by NASA's Earth Science Information Partnerships (ESIP): a federation of information sites for Earth science; and by the NOAA/NASA Pathfinder Program for early EOS products; principal investigator: Frank Wentz. The comments of two anonymous referees were very useful for improving this paper.

APPENDIX

a Computation of the local modes for one parameter

The LMA technique is based on a CEOF computation on a running time section (of 120 days here). For each time step (m) of the running analysis, only the *leading CEOF* is retained, corresponding to one particular pattern $\tilde{Z}_p^m(x)$ explaining a percentage of variance Π_p^m. Maxima in the Π_p^m time series are then identified and the *leading CEOF* of the time section corresponding to these maxima are called *Local Modes*. One can demonstrate that the spatial patterns $\tilde{Z}_p^m(x)$ of these *Local Modes* are more persistent in time and/or more spatially coherent than the patterns of other *leading CEOF* (Goulet and Duvel 2000).

Mathematically, for each time step (m), we consider the 120-day time series $S_p^m(x,t)$ of parameter (p), for each region (x) with $1 \le x \le N$ and $1 \le t \le T$ (T=120). The leading eigenvector is computed from the cross spectrum matrix $\tilde{\zeta}_p^m$ defined as:

$$\tilde{\zeta}_p^m(k,k') = \sum_{x=1}^{N} \tilde{F}_p^m(x,k)\, \tilde{F}_p^{m^*}(x,k') \qquad \text{(A1)}$$

where $\tilde{X}$ are complex numbers and $\tilde{X}^*$ their complex conjugate, k is the harmonic number (for the whole spectrum $1 \le k \le T/2$) and $\tilde{F}_p^m(x,k)$ represents the Fourier coefficients defined as:

$$\tilde{F}_p^m(x,k) = \frac{\sqrt{2}}{T} \sum_{t=1}^{T} w(t) S_p^m(x,t)\, e^{-2i\pi kt/T} \qquad \text{(A2)}$$

where w(t) is the Welch window. Since the Complex EOF has to be applied to a restricted time-spectral domain, $S_p(x,t)$ is filtered prior to the analysis and $\tilde{\zeta}_p^m$ can be computed on a restricted time-spectral band $[k_1, k_2]$ so that the dimension of the matrix is only $K_n \times K_n$ with $K_n = k_2 - k_1 + 1$. The leading eigenvectors of $\tilde{\zeta}_p^m$ is a complex normalized spectrum $\tilde{\psi}_p^m(k)$ from which we can retrieve the spatial eigenvectors $\tilde{Z}_p^m(x)$ by:

$$\tilde{Z}_p^m(x) = \sum_{k=k_1}^{k_2} \tilde{F}_p^m(x,k)\,\tilde{\psi}_p^{m^*}(k) \qquad \text{(A3)}$$

For a region x, the reconstructed time series associated with the local mode of the time step (m) is given by:

$$S_p^m(x,t) = A_p^m(x) B^m(t) \cos\left(\phi_p^m(x) + \chi^m(t)\right) \qquad \text{(A4)}$$

where $A_p^m(x) = \left|\tilde{Z}_p^m(x)\right|$ and $\phi_p^m(x) = Arg\left[\tilde{Z}_p^m(x)\right]$ are respectively the regional standard deviation and phase of the leading complex eigenvector $\tilde{Z}_p^m(x)$. $B^m(t)$ and χ (t) represents respectively the amplitude and phase obtained by inverse Fourier transform of $\tilde{\psi}_p^m(k)$. The summation of $A_p^m(x)^2$ over all regions is the variance of the leading CEOF. It is possible to define a Regional Representation Index $R_p^m(x)$ for the local mode m as:

$$R_p^m(x) = \frac{A_p^m(x)^2}{V_p^m(x)} \qquad \text{(A5)}$$

where,

$$V_p^m(x) = \sum_{k=k_1}^{k_2} \tilde{F}_p^m(x,k)\,\tilde{F}_p^{m^*}(x,k) \qquad \text{(A6)}$$

is the variance (weighted by the Welch window) of parameter (p) in the selected frequency band [k_1, k_2]. $R_p^m(x)$ represents for each region and the corresponding Local Mode the part of the regional intra-seasonal perturbation that is coherent at large scale. Note that the percentage of variance is also given by:

$$\Pi_p^m = \frac{\sum_{x=1}^{N} A_p^{m^2}(x)}{\sum_{x=1}^{N} V_p^m(x)} \qquad \text{(A7)}$$

b Multivariate analysis

This technique may be further used to study perturbations of a second parameter (q) associated

with the perturbation of the leading parameter (p). Indeed, the projection (Eq.A3) of the normalized spectrum $\tilde{\psi}_p^m(k)$ may be done with the Fourier coefficient $\tilde{F}_q^m(x,k)$ of another parameter (q). In such a case, the obtained $\tilde{Z}_{p,q}^m(x)$ represents the spatial pattern of the perturbation of (q) related to the large-scale organized perturbation of (p), through a "spectral key" $\tilde{\psi}_p^m(k)$. In other words, the distribution of amplitudes and phases of $\tilde{Z}_{p,q}^m(x)$ represents the part of the regional signal of (q) that is correlated with the large-scale organized perturbation of (p) represented by the Local Mode (m). As for the reference parameter (p), a Regional Representation Indexes $R_{p,q}^m(x)$ may be defined as

$$R_{p,q}^m(x) = \frac{A_{p,q}^{m\ 2}(x)}{V_q^m(x)} \qquad \text{(A8)}$$

c Average multivariate patterns

The average pattern is computed for the reference parameter from a cross spectrum matrix of dimension (N, N) where N is the number of regions, as described in Goulet and Duvel (2000). Each element of the matrix is an average cross spectrum computed from a given selection (an ensemble S) of Local Modes. For the present study, p is the OLR and the ensemble S is a particular season. This selection may be based on season or on another criterion. Each element of this mean cross spectrum matrix $\bar{\tilde{\zeta}}_{p,s}$ is defined as:

$$\bar{\tilde{\zeta}}_{p,s}(x,x') = \sum_{m \in S} \sum_{k=k_1}^{k_2} \tilde{L}_p^m(x,k)\, \tilde{L}_p^{m^*}(x',k) \qquad \text{(A9)}$$

where $\tilde{L}_p^m(x,k)$ is the spectrum for the parameter p and region x, corresponding to the Local Mode m:

$$\tilde{L}_p^m(x,k) = \tilde{Z}_p^m(x)\, \tilde{\psi}_p^m(k) \qquad \text{(A10)}$$

Note that the pattern obtained is generally very close (but the percentage of variance is

smaller) if one uses the original spectra $\tilde{F}_p^m(x,k)$ instead of the Local Mode spectra $\tilde{L}_p^m(x,k)$. Using the normalized first eigenvector $\tilde{Z}_{p,s}(x)$of the average cross-spectrum matrix $\overline{\overline{\tilde{\zeta}}}_{p,s}$, and the regional spectra $\tilde{L}_p^m(x,k)$ (or $\tilde{F}_p^m(x,k)$), the average spectrum $\tilde{\psi}_p^y(k)$ for each Local Mode window (m) is given by:

$$\tilde{\psi}_{p,s}^m(k) = \sum_x \tilde{F}_p^m(x,k)\,\tilde{Z}_{p,s}^*(x) \tag{A11}$$

These spectra are then normalized such that:

$$\sum_{m\in S}\sum_{k=k_1}^{k_2}\left|\tilde{\psi}_{p,s}^m(k)\right|^2 = 1 \tag{A12}$$

Then, for each parameter q, an average pattern corresponding to these spectra (that are spectral keys corresponding to the average pattern of the reference parameter) can be computed from the spectra $\tilde{L}_q^m(x,k)$ (or $\tilde{F}_q^m(x,k)$):

$$\tilde{Z}_{q,s}^p(x) = \sum_{m\in S}\sum_{k=k_1}^{k_2}\tilde{L}_q^m(x,k)\,\tilde{\psi}_{p,s}^{m\,*}(k) \tag{A13}$$

These are the average patterns of the perturbation of the parameter q associated to the *large-scale organized perturbations of the reference parameter* p (one may verify that $\tilde{Z}_{p,s}^p(x)=\tilde{Z}_{p,s}(x)$). These patterns are used in section 4 to analyse the average relation between the OLR, the SST and the surface wind intraseasonal perturbations. Since the normalized spectra $\tilde{\psi}_{p,s}^m(k)$ are not from parameter q, the principal component time series corresponding to $\tilde{Z}_{q,s}^p(x)$ and the corresponding variance (and percentage of variance) has to be computed by a projection of the $\tilde{L}_q^m(x,k)$ (or $\tilde{F}_q^m(x,k)$) on $\tilde{Z}_{q,s}^p(x)$.

The LMA makes it possible to measure the resemblance between an average pattern and the patterns for each Local Mode. This is very important to verify if this average pattern is only a mathematical object or if it is representative of the different events, i.e. if it is appropriate to give

a physical interpretation of the average pattern. As in Goulet and Duvel (2000), this resemblance is computed as a normalized distance between the complex eigenvectors representing the average pattern $\tilde{Z}^{p}_{q,s}(x)$ and the pattern of each Local Mode $\tilde{Z}^{m}_{q}(x)$. A normalized distance of 0 means that the patterns are identical and a normalized distance of one means that the two patterns are orthogonal.

References

Anderson, S. P., R. A. Weller, and R. Lukas, 1996 : Surface buoyancy forcing and the mixed layer of the western Pacific warm pool: Observations and 1D model results. *J. Climate*, **9**, 3056-3085.

Bhat, G. S., G. A. Vecchi and S. Gadgil. 2004: Sea Surface Temperature of the Bay of Bengal Derived from the TRMM Microwave Imager. *J. Atmos. Oceanic Technol.*, **21**, 1283–1290.

Chelton, D.B., F.J. Wentz, C.L. Gentemann, R.A. de Skoeze and M.G. Schlax, Satellite microwave SST observations of transequatorial tropical instability waves, *Geophys. Res. Lett.,* **27,** 1239-1242, 2000.

de Boyer Montégut C., G. Madec, A. S. Fischer, A. Lazar, and D. Iudicone, 2004: Mixed layer depth over the global ocean: an examination of profile data and a profile-based climatology, *J. Geophys. Res*., **109**, C12003, doi:10.1029/2004JC002378.

Duvel, J-P., R. Roca and J. Vialard, 2004: Ocean Mixed Layer Temperature Variations induced by Intraseasonal Convective Perturbations over the Indian Ocean. *J. Atmos. Sci.*, **61**, 1004-1023.

Flatau, M. K. , P. J. Flatau and D. Rudnick. 2001: The Dynamics of Double Monsoon Onsets. *J. Climate*, **14**, 4130–4146.

Gill, A. E., 1980: Some simple solutions for heat-induced tropical circulation. *Quart. J. Roy. Meteor. Soc.*, **106**, 447–462.

Goswami, B. N., and R. S. Ajaya Mohan, 2001: Intraseasonal oscillations and interannual variability of the Indian summer monsoon. *J. Climate*, **14**, 1180–1198.

Goulet, L., and J-P. Duvel, 2000: A New Approach to Detect and Characterize Intermittent Atmospheric Oscillations: Application to the Intraseasonal Oscillation. *J. Atmos. Sci.*, **57**, 2397–2416.

Harrison, D.E., and A. Vecchi, 2001: January 1999 Indian Ocean cooling event. *Geophys. Res. Let.*, **28**, 3717-3720.

Hasselman, K., 1976 : Stochastic climate models. 1 : Theory. *Tellus* **28,** 473-485.

Inness, P. M., and J. M. Slingo, 2003: Simulation of the Madden–Julian Oscillation in a Coupled General Circulation Model. Part I: Comparison with Observations and an Atmosphere-Only GCM. *J. Climate*, **16**, 345–364.

Jones, C., D. E. Waliser, C. Gautier, 1998: The Influence of the Madden–Julian Oscillation on Ocean Surface Heat Fluxes and Sea Surface Temperature. *J. Climate*, **11**, 1057–1072.

Joseph, P. V., S. Sijikumar 2004: Intraseasonal Variability of the Low-Level Jet Stream of the Asian Summer Monsoon. *J. Climate*, **17**, 1449-1458.

Kanamitsu, M., Ebisuzaki, W., Woollen, J., Yang, S.-K., Hnilo, J.J., Fiorion, M. and Potter, G.L., 2002: NCEP-DOE AMIP-II Reanalysis (R-2). *Bull. Amer. Meteorol. Soc.,* 83, 1631 - 1643.

Kawamura, R, 1988 : Intraseasonal Variability of Sea Surface Temperature over the Tropical Western Pacific, *J. Meteor. Soc. Japan*, **66**, 1007-1012.

Kindle, J.C. and J.D. Thompson, 1989: 26 and 50-day period oscillations in the Indian Ocean: Model results. *J. Geophys. Res.,* **94,** 4721-4736.

Lawrence, D. M., and P. J Webster,. 2002: The Boreal Summer Intraseasonal Oscillation: Relationship between Northward and Eastward Movement of Convection. *J. Atmos. Sci.*, **59**, 1593–1606.

Lengaigne, M., J.-P. Boulanger , C. Menkes, S. Masson, P. Delecluse et G. Madec, Ocean response to the March 1997 westerly wind event, *J. Geophys. Res.,* **107**, 2002.

Liebmann, B., and C.A. Smith, 1996: Description of a complete (Interpolated) Outgoing Longwave Radiation Dataset, *Bull. Amer. Meteor. Soc.,* **77**, 1275-1277.

Madden, R.A., and P.R. Julian, 1994: Observations of the 40-50 day tropical oscillation - A review, *Month. Wea. Rev,* **122**, 814-836.

Maloney, E.D. and A. H. Sobel. 2004: Surface Fluxes and Ocean Coupling in the Tropical Intraseasonal Oscillation. *J. Climate,* **17**, 4368–4386.

McPhaden, M. J., 1999: Genesis and evolution of the 1997-1998 El Niño, *Science*, **283**, 950-954.

Reynolds, R. W., T. M. Smith, 1994: Improved Global Sea Surface Temperature Analyses Using Optimum Interpolation**.** *J. Climate,* **7**, 929–948.

Sengupta, D., and M. Ravichandran, 2001: Oscillations of Bay of Bengal sea surface temperature during the 1998 summer monsoon, Geophys. Res. Lett., **28**, 2033-2036.

Sengupta, D., B.N. Goswami, and R. Senan, 2001: Coherent intraseasonal oscillations of ocean and atmosphere during the asian summer monsoon, *Geophys. Res. Let.*, **28**, 4127-4130.

Shinoda, T., and H. H. Hendon, 1998: Mixed Layer Modeling of Intraseasonal Variability in the Tropical Western Pacific and Indian Oceans. *J. Climate,* **11**, 2668–2685.

Shinoda, T., and H. H. Hendon, 2001: Upper-Ocean Heat Budget in Response to the Madden–Julian Oscillation in the Western Equatorial Pacific. *J. Climate,* **14**, 4147–4165.

Shinoda, T., H. H. Hendon, J. Glick, 1998: Intraseasonal Variability of Surface Fluxes and Sea Surface Temperature in the Tropical Western Pacific and Indian Oceans. *J. Climate,* **11**, 1685–1702.

Tsai, P.T.H., J.J. O'Brien, M.E. Luther, The 26-day oscillation observed in the satellite sea surface temperature measurements in the equatorial western Indian Ocean. *J. Geophys Res.,* **31,** 9605-9618, 1992.

Vecchi, G.A., and D.E. Harrison, 2002: Monsoon Breaks and Subseasonal Sea Surface Temperature Variability in the Bay of Bengal, *J. Climate,* **15**, 1485-1493

Waliser, D. E., K. M. Lau, J.-H. Kim, 1999: The Influence of Coupled Sea Surface Temperatures on the Madden–Julian Oscillation: A Model Perturbation Experiment. *J. Atmos. Sci.*, **56**, 333–358.

Webster P. J., A. M. Moore, J. P. Loschnigg and R. Leben, 1999: Coupled ocean – atmosphere dynamics in the Indian ocean during 1997 – 98, *Nature*, **401**, 356-360.

Webster, P. J., V. O. Magana, T. N. Palmer,J. Shukla, R.A. Tomas, M. Yanai, T. Yasunari,

1998: Monsoons: Processes, predictability, and the prospects for prediction, *J. Geophys. Res.*, **103**, C7, 14451-14510.

Weller, R.A., and S.P. Anderson, 1996: Surface Meteorology and Air-Sea Fluxes in the Western Equatorial Pacific Warm Pool during the TOGA Coupled Ocean-Atmosphere Response Experiment. *J. Climate*, **9**, 1959–1992.

Wentz,F.J., C. Gentemann, D.Smith, D.Chelton, 2000: Satellite measurements of sea-surface temperature through clouds. *Science,* **288**, 847-850.

Woolnough, S. J., J. M. Slingo, B. J. Hoskins, 2000: The Relationship between Convection and Sea Surface Temperature on Intraseasonal Timescales. *J. Climate,* **13**, 2086–2104.

Zhang, C., and M. Dong. 2004: Seasonality in the Madden–Julian Oscillation. *J. Climate*, **17**, 3169–3180.

Figure Captions

Figure 1: Standard deviation of the SST in the 20-90 day band on the average for years 1998-2004 for (a) the SST-TMI dataset and (b) the Reynolds and Smith SST dataset.

Figure 2: Standard deviation $A_p^m(x) = \left|\tilde{Z}_p^m(x)\right|$ and relative phase $\phi_p^m(x) = Arg\left[\tilde{Z}_p^m(x)\right]$ of the event extracted from the Local Mode Analysis for summer 2000 for (a) the OLR signal as the leading parameter, (b) for the OLR-related event for the SST and (c) for the OLR-related event for the surface wind. The segment length is proportional to the standard deviation and the angle of the segment represents the relative phase of the quasi-periodic signal. A relative phase difference of π between regions or between parameters represents a lag of about 15 days between maxima. The angle increases clockwise with time (e.g. northward propagation for a segment rotating clockwise toward the north). The contour lines represent a RRI (Eq.A5 and A8) of 0.6 (dotted) and 0.8 (solid).

Figure 3: (a) Reconstructed signals (Eq.A4) for the event of figure 1 and for the region 15°N – 87.5°E, for the OLR (left axis in Wm^{-2}), the SST (right axis in K) and the surface wind (inside right axis in ms^{-1}). This reconstructed signal is superimposed to the raw signal for (b) OLR, (c) SST and (d) surface wind. (e) Time evolution of the variance percentage (Eq.A7) for each time step (m) and each parameter; larger markers correspond to the local maximum of the variance percentage for the OLR (leading parameter) and thus to the central date of the time window for this Local Mode of summer 2000.

Figure 4: Seasonal (JFM, JJA) average (contours) and 20-90 day band standard deviation (colors) for (a, e) the NOAA-OLR, (b, f) the NCEP surface wind module and, (c, g). the TMI SST. (d, h). Seasonal average of the mixed layer depth from the de Boyer Montégut (2004) climatology.

Figure 5: (Left) Correlation between the derivative of the TMI-SST and the NCEP net surface fluxes for (a) the 30-90 day band in JFM, (b) the 20-30 day band in JFM, (c) the 30-90 day band in JJA and, (d) the 20-30 day band in JJA. (Right) Scatter diagrams for regions with a correlation coefficient larger than 0.5 of σ_T^{ω} and σ_Q^{ω}/H and linear regression line for (e) the 30-90 day band in JFM, (f) the 20-30 day band in JFM, (g) the 30-90 day band in JJA and,

(h) the 20-30 day band in JJA. The value of the slope c, the corresponding time-scale (τ) and the linear correlation coefficient (Pr) are also indicated in figures (e) to (h).

Figure 6: Monthly statistics of the intraseasonal events over the Indian Ocean area for (a) the average standard deviation of the Local Modes and, (b) the average time-scale (or period) of each Local Mode. The markers represent the year unit between 199(8)-200(4) of each event.

Figure 7: Multivariate average pattern of intraseasonal variation of the OLR (top), the SST (middle) and the surface wind (bottom) for, from left to right, the January-March season (7 events), May (6 events) and the June-August season (10 events). The corresponding variance percentages for each parameter and each season are reported in the figure. The segment length is proportional to the standard deviation and the angle of the segment represents the relative phase. The angle increases clockwise with time (e.g. northward propagation for a segment rotating clockwise toward the north). The contour lines represent the standard deviation of these average patterns.

Figure 8: Phase difference between the SST perturbation and the OLR (top), between the SST perturbation and the surface wind (middle) and between the OLR and the surface wind (bottom) for the three considered seasons. For the top figures, a northward (eastward) pointer means that the OLR is minimal 1/4 of period before (simultaneous with) the minimum SST. For the middle graphs, a southward (westward) pointer means that the surface wind is maximal 1/4 of period before (simultaneous with) the minimum SST. For the bottom graphs, a southward (westward) pointer means that the surface wind is maximal 1/4 of period after (simultaneous with) the minimum OLR. The segment length is proportional to the product of normalized standard deviations of both considered parameters.

Figure 9: Normalized distance between the average multivariate patterns of figure 6 and the individual Local Modes patterns for the OLR (solid), the SST (dashed) and the module of the surface wind (dotted). The markers represent the Local Modes for the corresponding season. A small distance means that the Local Mode has a pattern similar to the seasonal average pattern.

Figure 10: As in figure 6 but for the Maritime Continent area.

Figure 11: As in figure 7 but for JFM and JJA over the Maritime continent and for JFM over the west Pacific Ocean.

Figure 12: As in figure 8 but for JFM and JJA over the Maritime continent and for JFM over the west Pacific Ocean.

Figure 13: As in figure 9 but for the Maritime Continent area.

Figure 14: As in figure 6 but for the Western Pacific area.

Figure 15: As in figure 9 but for the Western Pacific area.

Figure 16: Selected regions for the study the response of wind and SST to large-scale organised OLR perturbation for each intraseasonal event.

Figure 17: Relative delay between minimum OLR (square) and minimum SST (circle) and between minimum OLR and the maximum surface wind (triangle) for the 5 selected regions defined in figures 6 and 11 and for the January-March season for regions SW, SC and SE and the June-August season for region BB and May for region EQ. The size of the marker is proportional to the local amplitude of the event for each parameter. For each region, the smoothed time-series for the average OLR (solid, second left axis), SST (filled in grey, right axis) and surface wind (dotted; first left axis) are also shown.

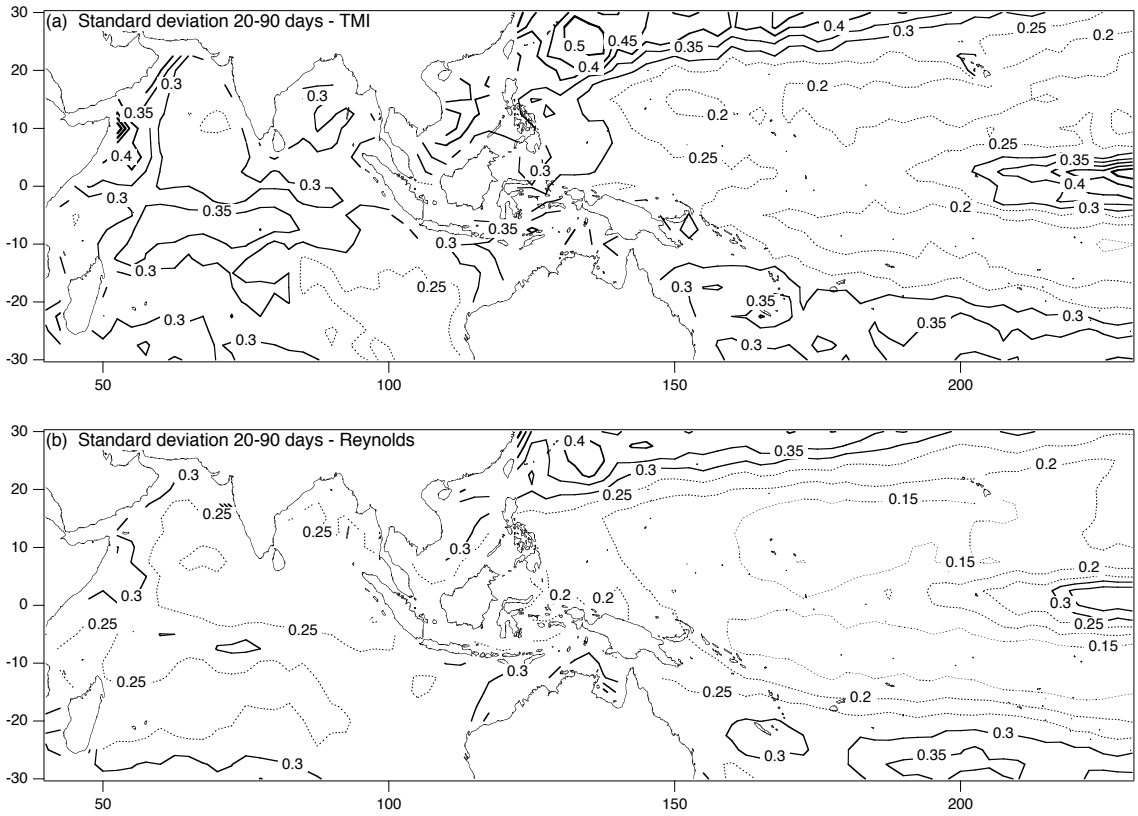

Figure 1: Standard deviation of the SST in the 20-90 day band on the average for years 1998-2004 for (a) the SST-TMI dataset and (b) the Reynolds and Smith SST dataset.

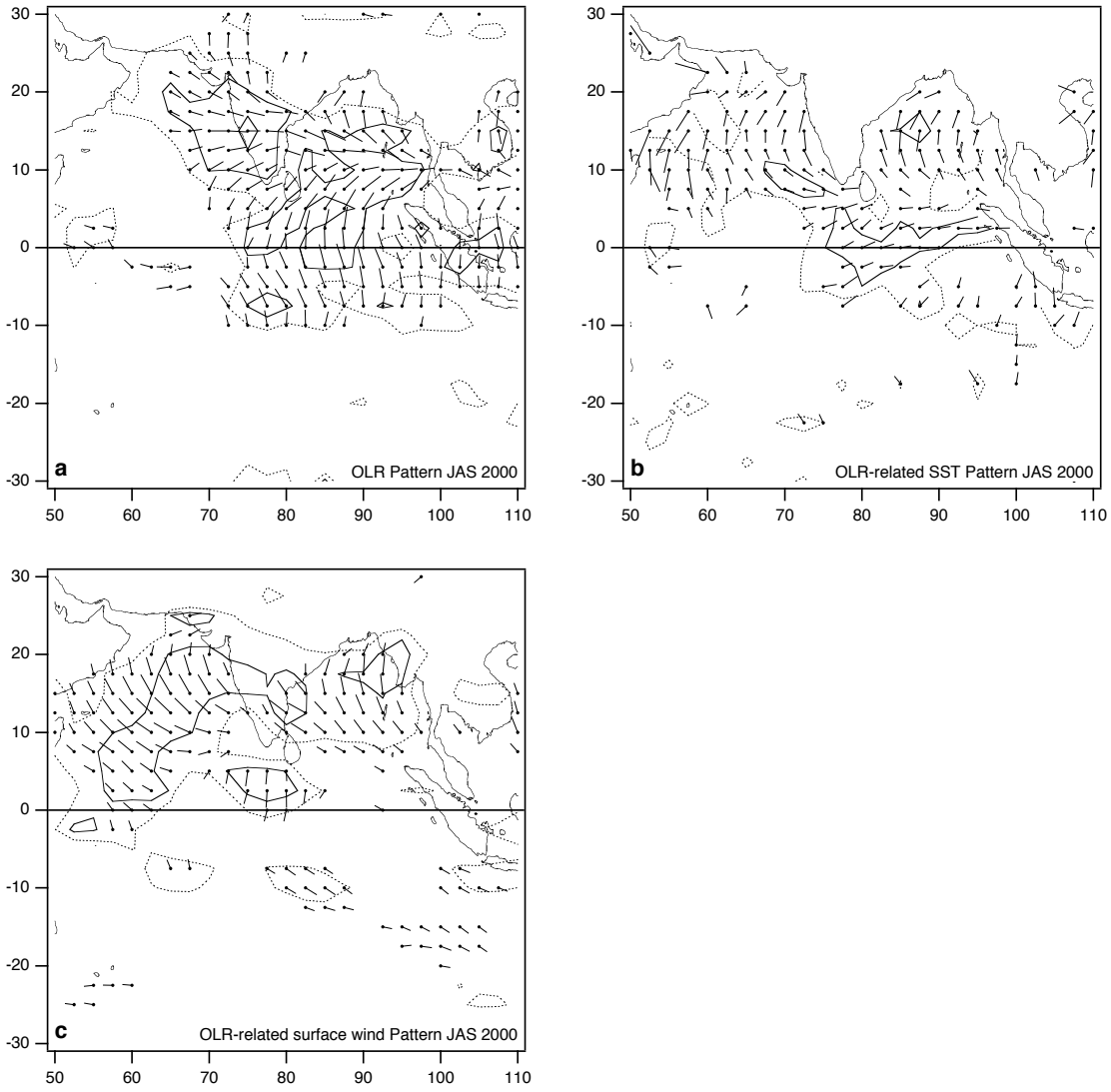

Figure 2: Standard deviation $A_p^m(x) = \left|\tilde{Z}_p^m(x)\right|$ and relative phase $\phi_p^m(x) = Arg\left[\tilde{Z}_p^m(x)\right]$ of the event extracted from the Local Mode Analysis for summer 2000 for (a) the OLR signal as the leading parameter, (b) for the OLR-related event for the SST and (c) for the OLR-related event for the surface wind. The segment length is proportional to the standard deviation and the angle of the segment represents the relative phase of the quasi-periodic signal. A relative phase difference of π between regions or between parameters represents a lag of about 15 days between maxima. The angle increases clockwise with time (e.g. northward propagation for a segment rotating clockwise toward the north). The contour lines represent a RRI (Eq.A5 and A8) of 0.6 (dotted) and 0.8 (solid).

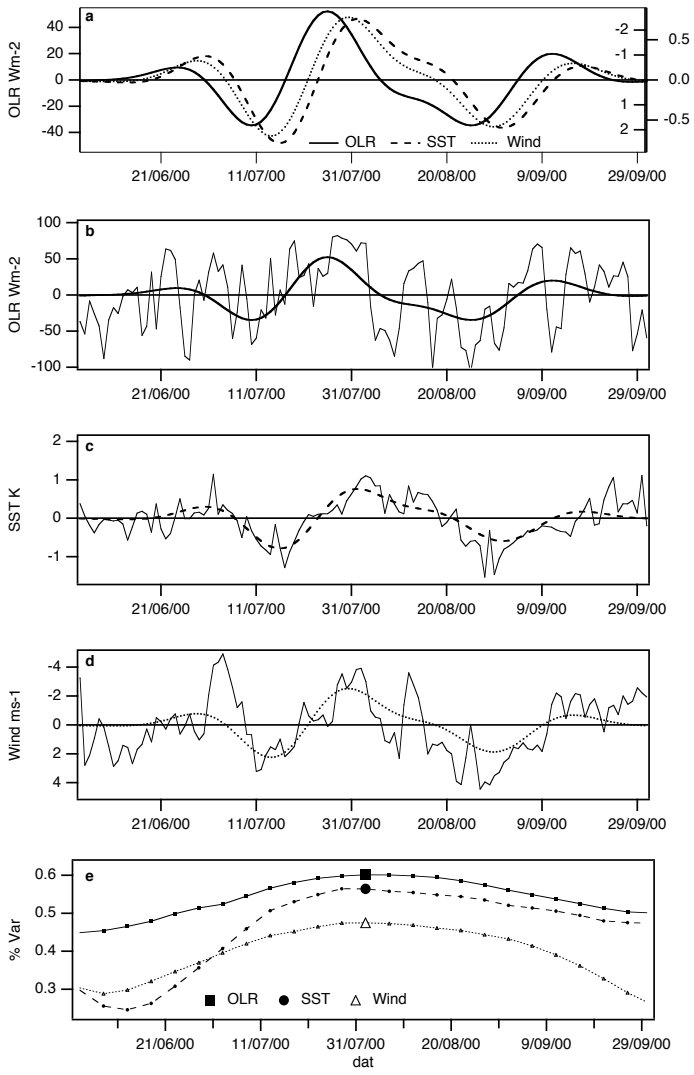

Figure 3: (a) Reconstructed signals (Eq.A4) for the event of figure 1 and for the region 15°N – 87.5°E, for the OLR (left axis in Wm^{-2}), the SST (right axis in K) and the surface wind (inside right axis in ms^{-1}). This reconstructed signal is superimposed to the raw signal for (b) OLR, (c) SST and (d) surface wind. (e) Time evolution of the variance percentage (Eq.A7) for each time step (m) and each parameter; larger markers correspond to the local maximum of the variance percentage for the OLR (leading parameter) and thus to the central date of the time window for this Local Mode of summer 2000.

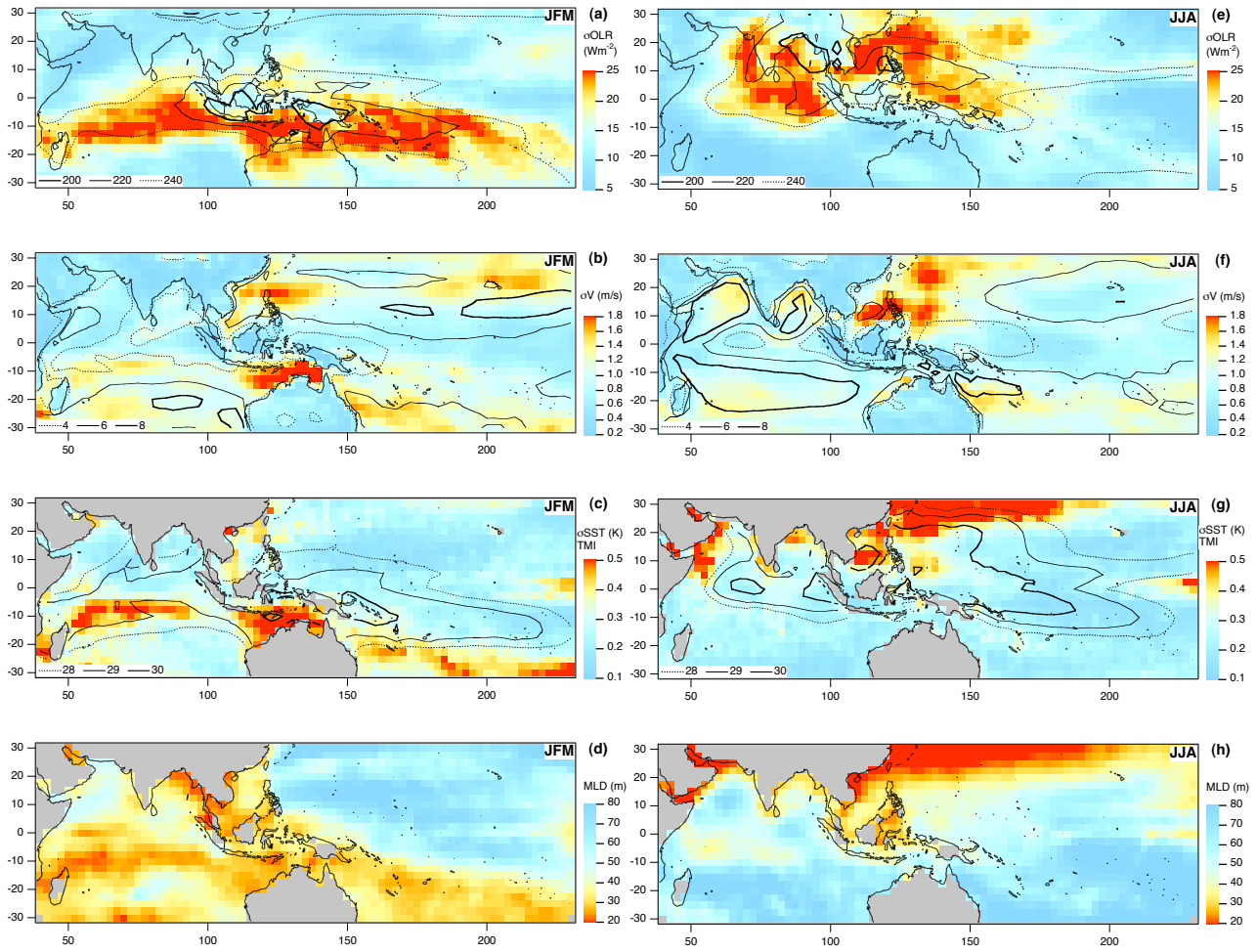

Figure 4: Seasonal (JFM, JJA) average (contours) and 20-90 day band standard deviation (colors) for (a, e) the NOAA-OLR, (b, f) the NCEP surface wind module and, (c, g). the TMI SST. (d, h). Seasonal average of the mixed layer depth from the de Boyer Montégut (2004) climatology.

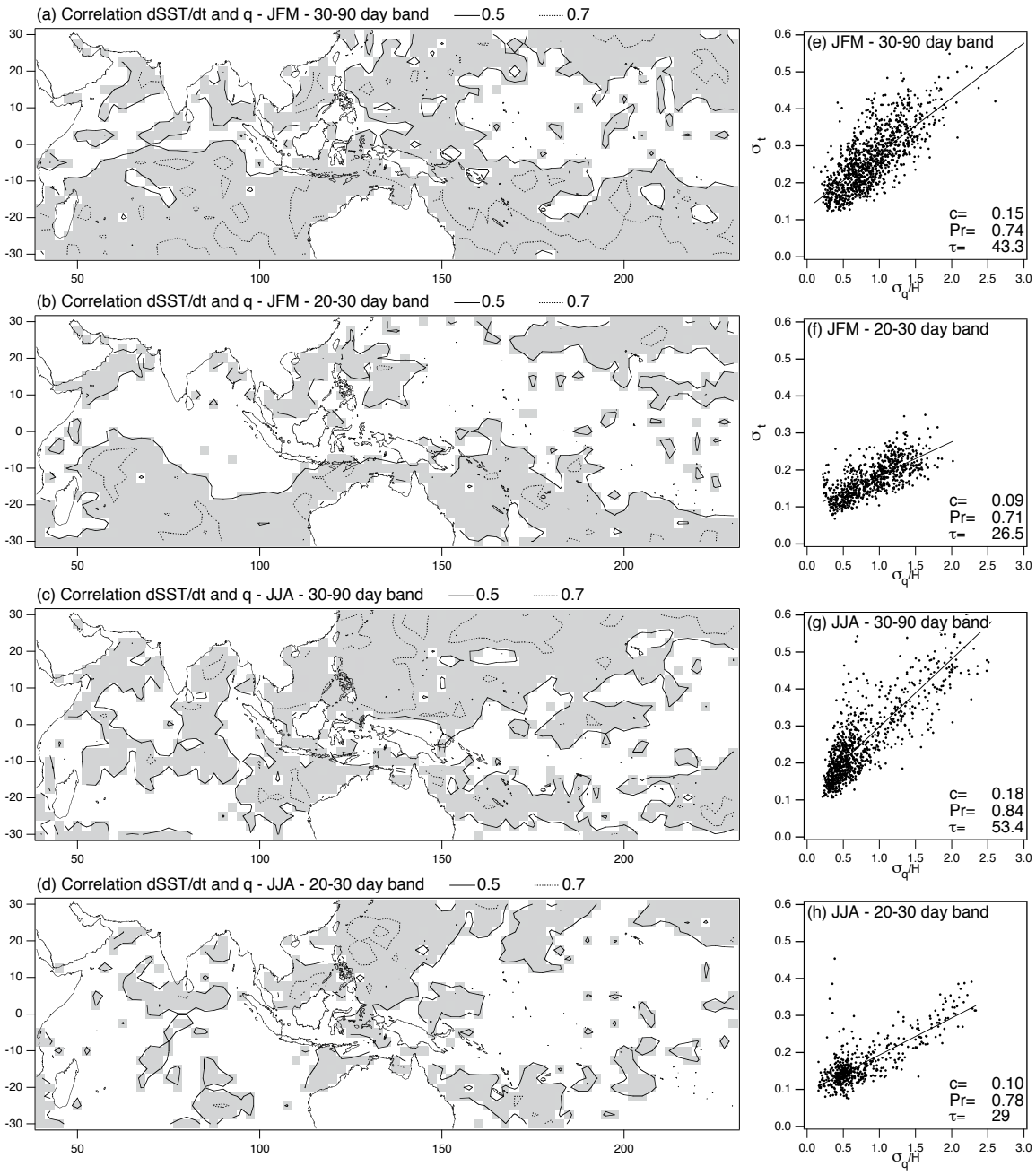

Figure 5: (Left) Correlation between the derivative of the TMI-SST and the NCEP net surface fluxes for (a) the 30-90 day band in JFM, (b) the 20-30 day band in JFM, (c) the 30-90 day band in JJA and, (d) the 20-30 day band in JJA. (Right) Scatter diagrams for regions with a correlation coefficient larger than 0.5 of σ_T^{ω} and σ_Q^{ω}/H and linear regression line for (e) the 30-90 day band in JFM, (f) the 20-30 day band in JFM, (g) the 30-90 day band in JJA and, (h) the 20-30 day band in JJA. The value of the slope c, the corresponding time-scale (τ) and the linear correlation coefficient (Pr) are also indicated in figures (e) to (h).

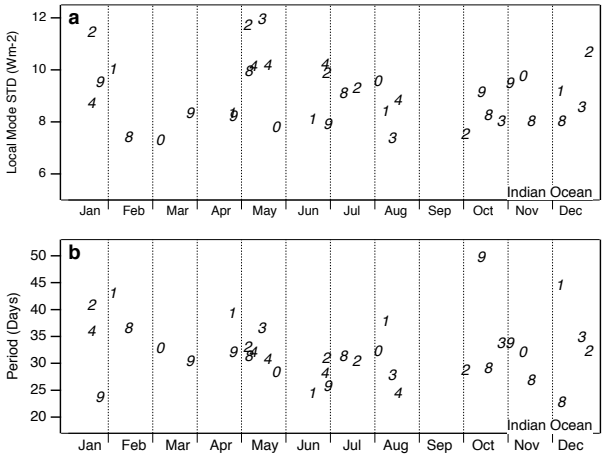

Figure 6: Monthly statistics of the intraseasonal events over the Indian Ocean area for (a) the average standard deviation of the Local Modes and, (b) the average time-scale (or period) of each Local Mode. The markers represent the year unit between 199(8)-200(4) of each event.

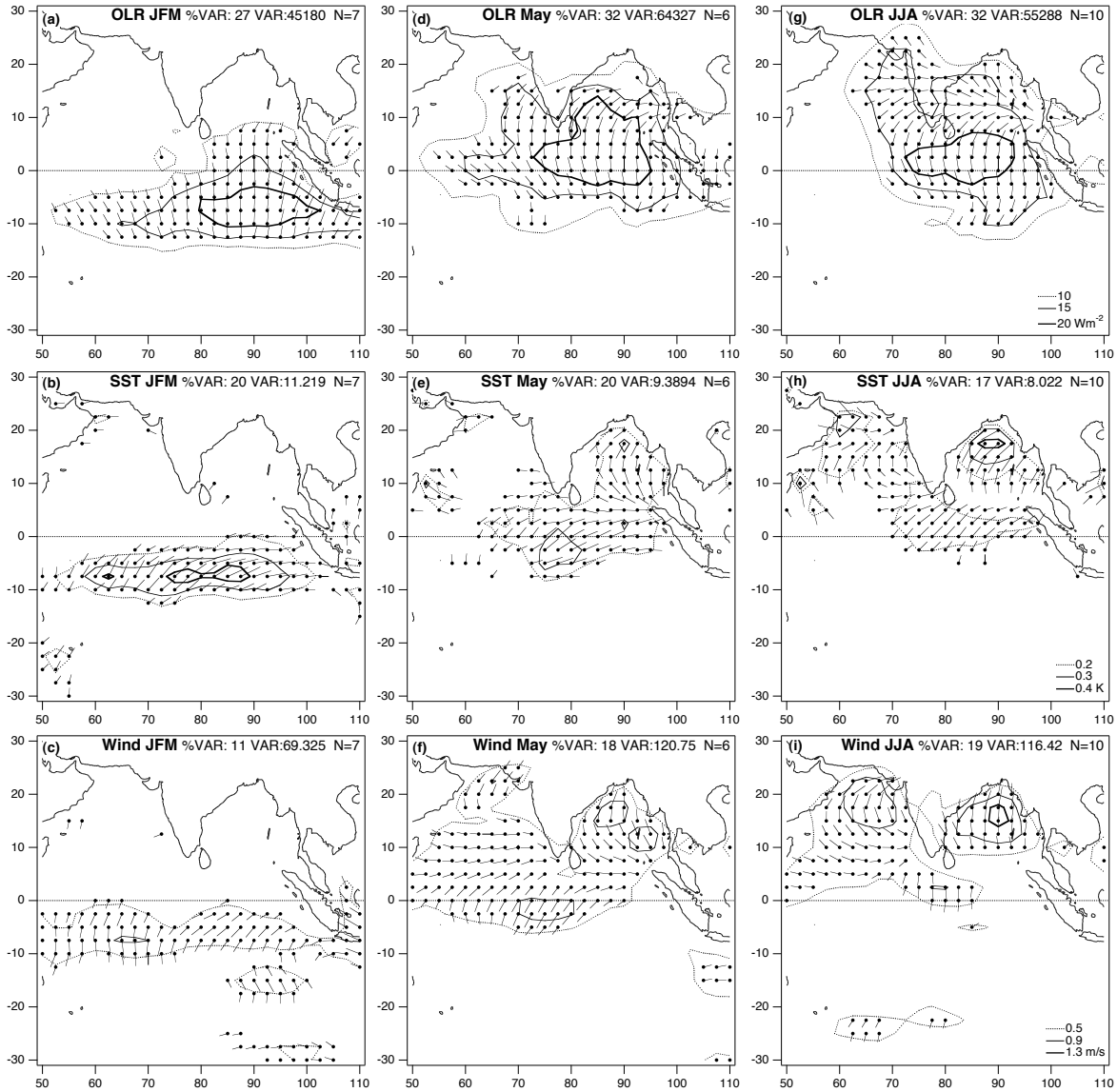

Figure 7: Multivariate average pattern of intraseasonal variation of the OLR (top), the SST (middle) and the surface wind (bottom) for, from left to right, the January-March season (7 events), May (6 events) and the June-August season (10 events). The corresponding variance percentages for each parameter and each season are reported in the figure. The segment length is proportional to the standard deviation and the angle of the segment represents the relative phase. The angle increases clockwise with time (e.g. northward propagation for a segment rotating clockwise toward the north). The contour lines represent the standard deviation of these average patterns.

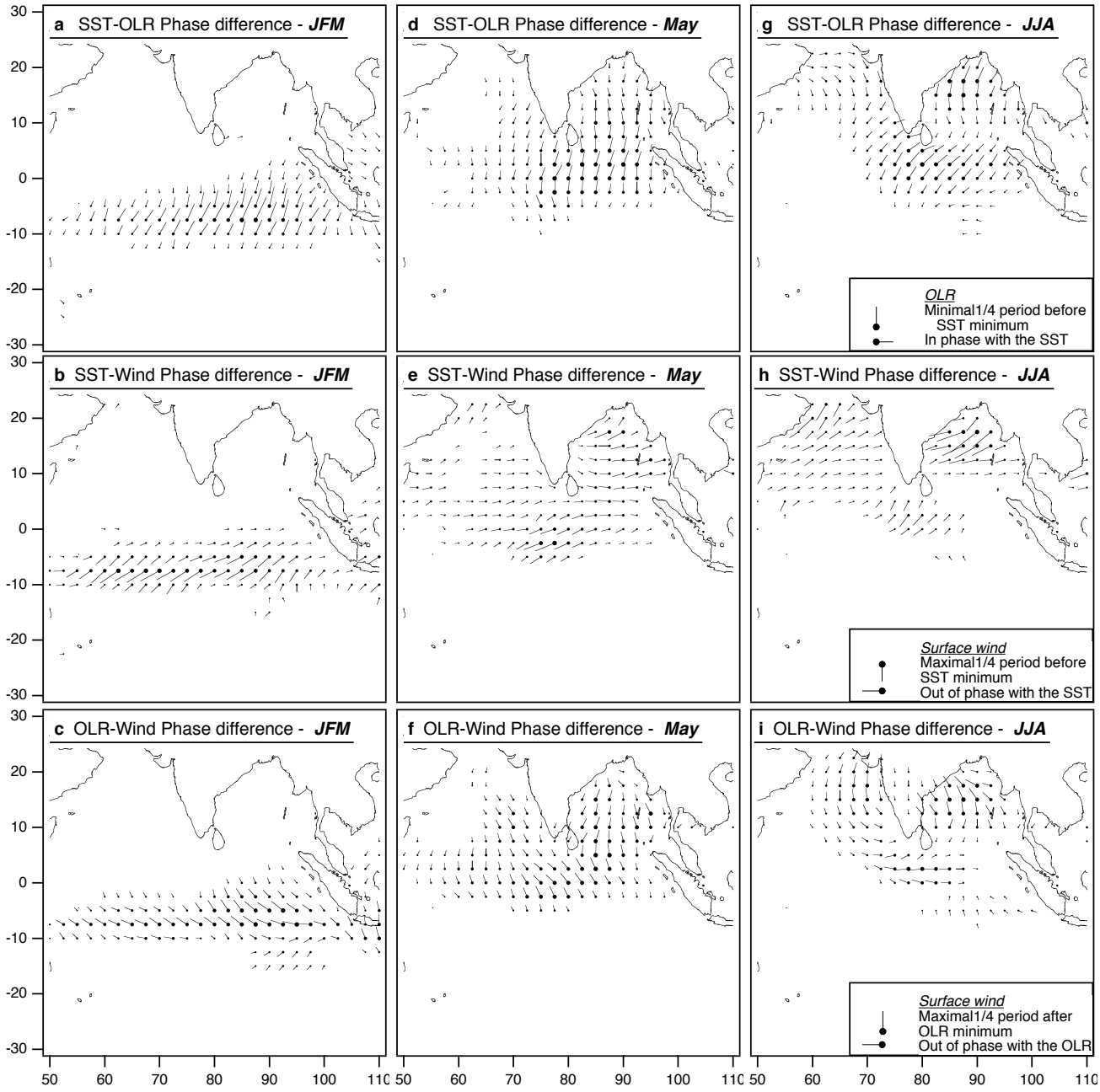

Figure 8: Phase difference between the SST perturbation and the OLR (top), between the SST perturbation and the surface wind (middle) and between the OLR and the surface wind (bottom) for the three considered seasons. For the top figures, a northward (eastward) pointer means that the OLR is minimal 1/4 of period before (simultaneous with) the minimum SST. For the middle graphs, a southward (westward) pointer means that the surface wind is maximal 1/4 of period before (simultaneous with) the minimum SST. For the bottom graphs, a southward (westward) pointer means that the surface wind is maximal 1/4 of period after (simultaneous with) the minimum OLR. The segment length is proportional to the product of normalized standard deviations of both considered parameters.

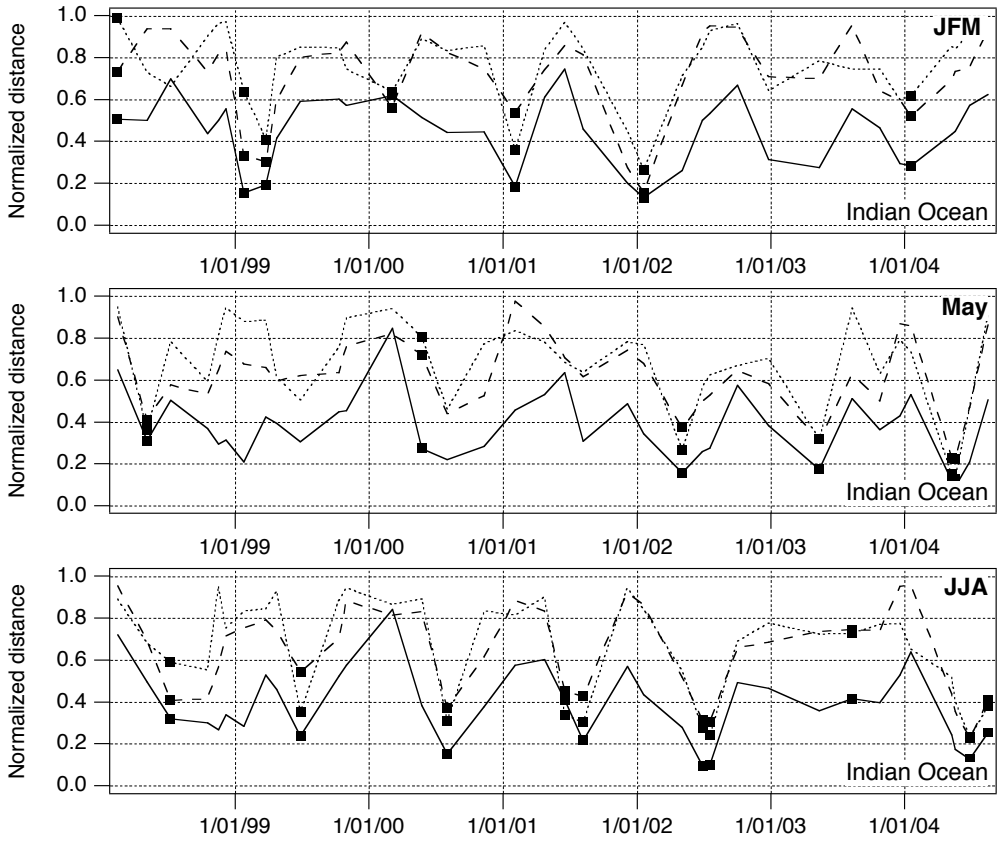

Figure 9: Normalized distance between the average multivariate patterns of figure 6 and the individual Local Modes patterns for the OLR (solid), the SST (dashed) and the module of the surface wind (dotted). The markers represent the Local Modes for the corresponding season. A small distance means that the Local Mode has a pattern similar to the seasonal average pattern.

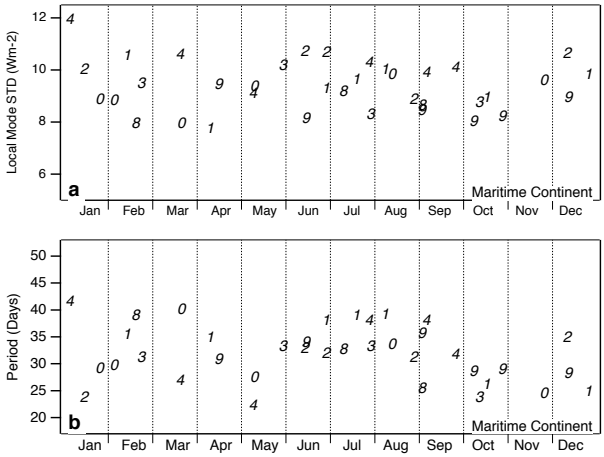

Figure 10: As in figure 6 but for the Maritime Continent area.

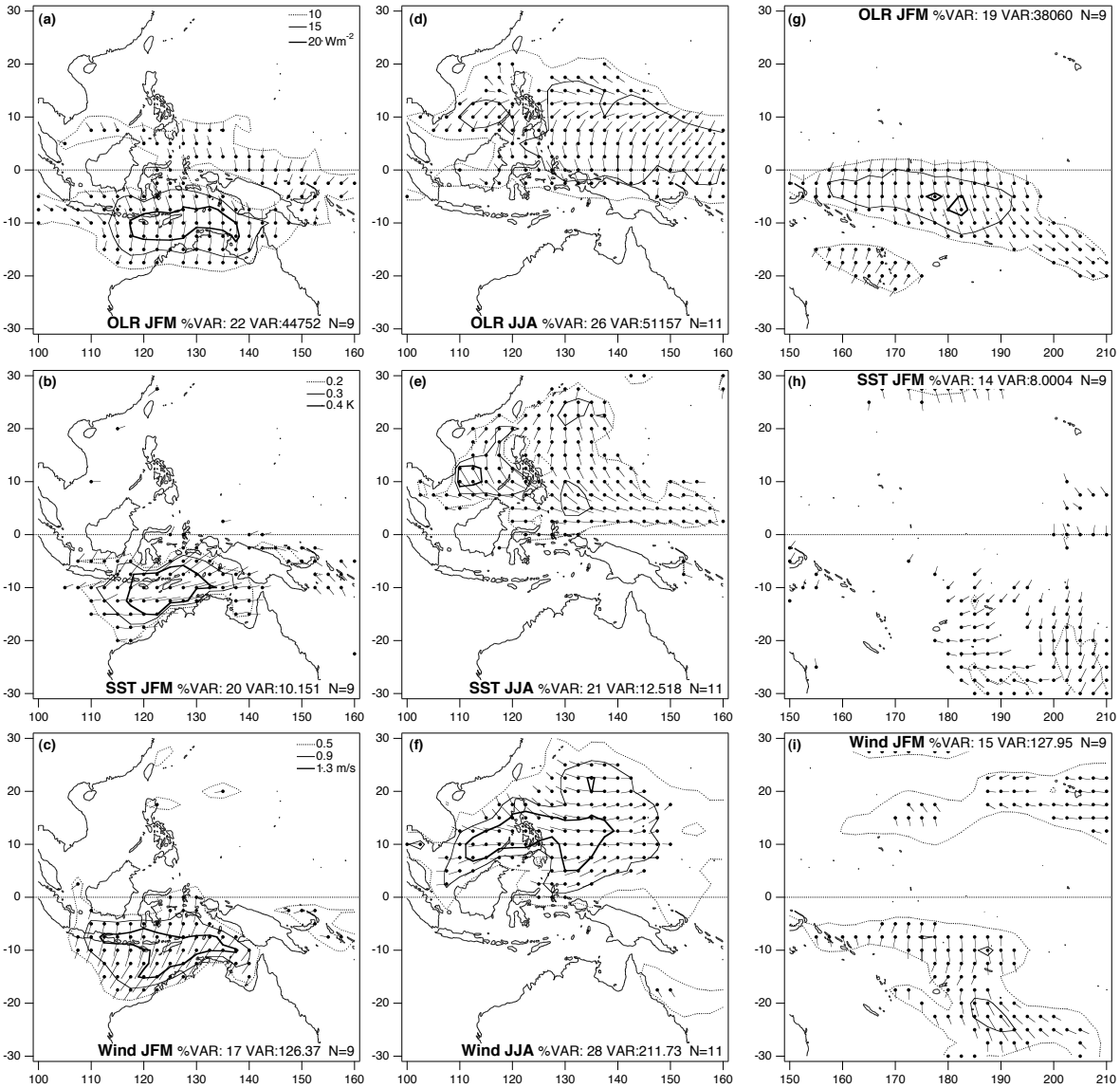

Figure 11: As in figure 7 but for JFM and JJA over the Maritime continent and for JFM over the west Pacific Ocean.

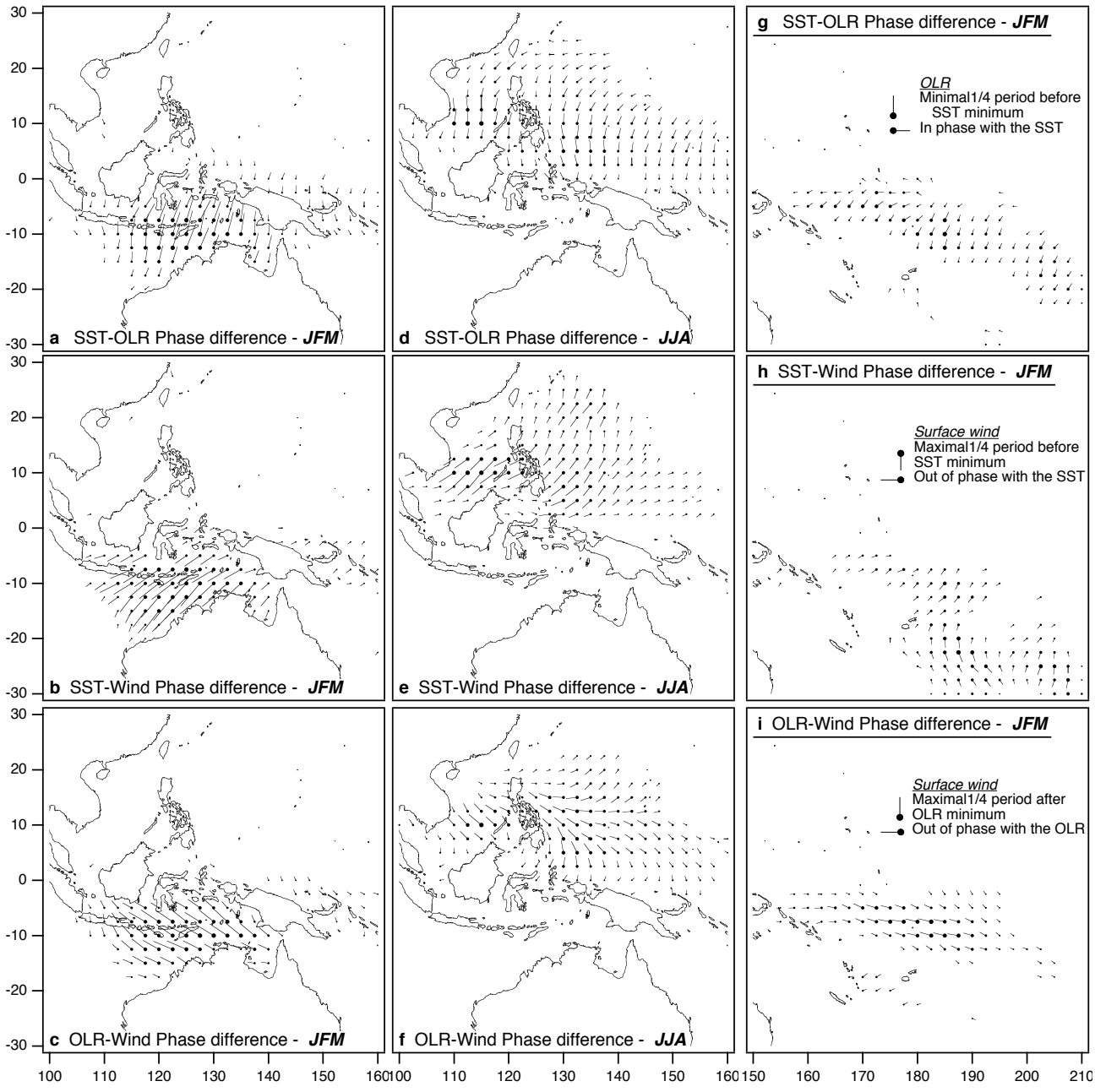

Figure 12: As in figure 8 but for JFM and JJA over the Maritime continent and for JFM over the west Pacific Ocean.

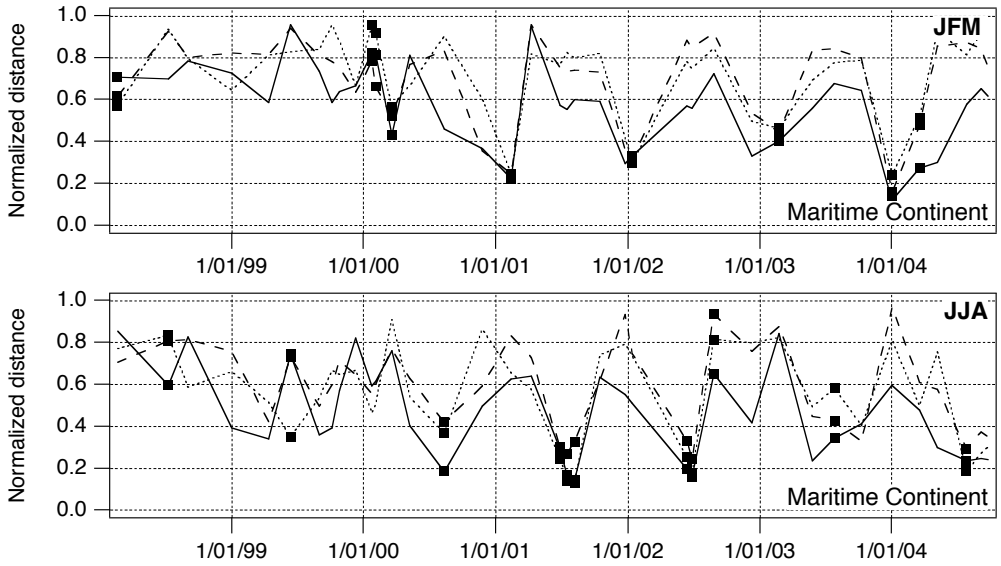

Figure 13: As in figure 9 but for the Maritime Continent area.

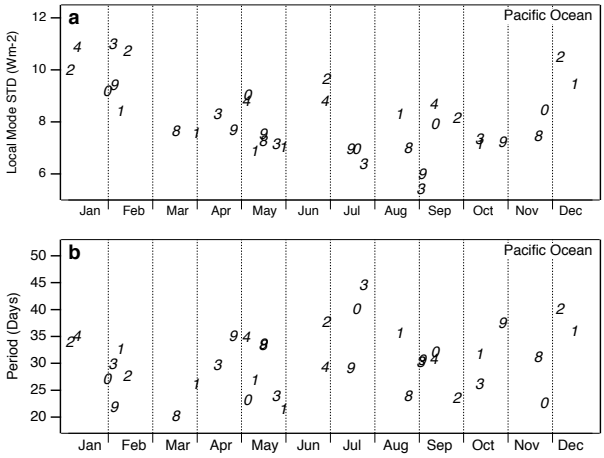

Figure 14: As in figure 6 but for the Western Pacific area.

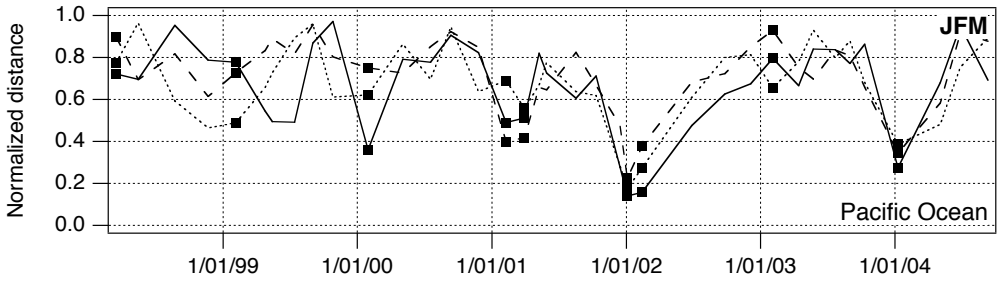

Figure 15: As in figure 9 but for the Western Pacific area.

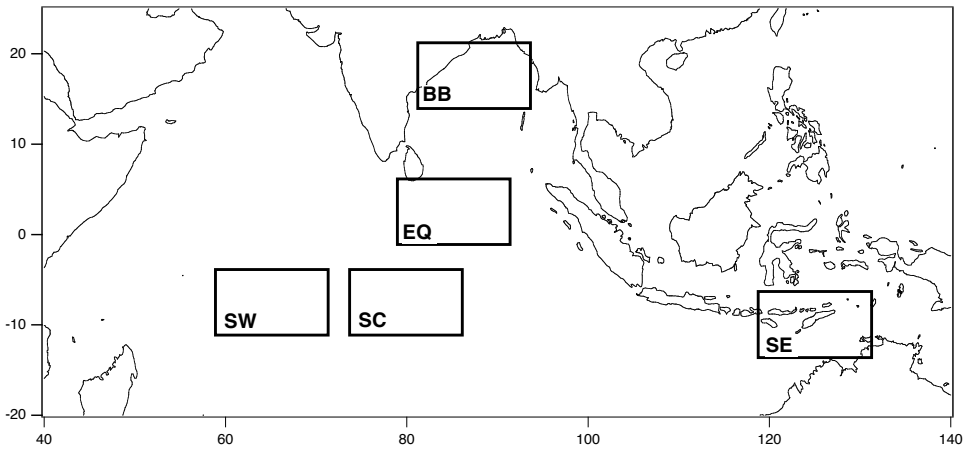

Figure 16: Selected regions for the study the response of wind and SST to large-scale organised OLR perturbation for each intraseasonal event.

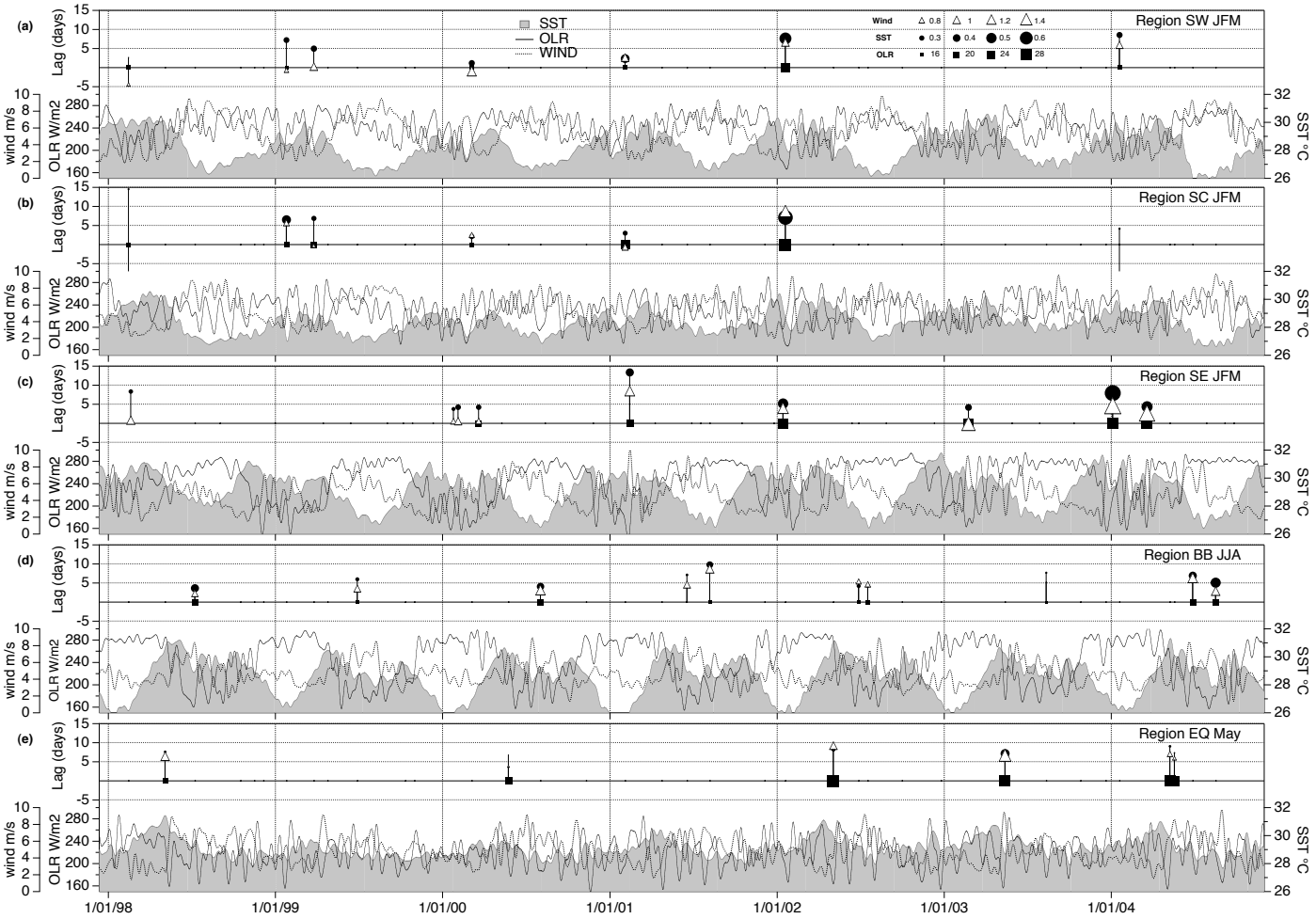

Figure 17: Relative delay between minimum OLR (square) and minimum SST (circle) and between minimum OLR and the maximum surface wind (triangle) for the 5 selected regions defined in figures 6 and 11 and for the January-March season for regions SW, SC and SE and the June-August season for region BB and May for region EQ. The size of the marker is proportional to the local amplitude of the event for each parameter. For each region, the smoothed time-series for the average OLR (solid, second left axis), SST (filled in grey, right axis) and surface wind (dotted; first left axis) are also shown.